future transportation

MDPI

Article

Exploring Spatial Variations in Factors Influencing Cyclist Injury Severity in Traffic Crashes: A Comparison of Geographically Weighted Regression and Spatial Machine Learning

Yanfang Su [1], Zihe Zhang [2,*], Jun Liu [1,†], Emmanuel Kofi Adanu [1] and Steven Jones [1,2]

[1] Department of Civil, Construction, and Environmental Engineering, The University of Alabama, Tuscaloosa, AL 35487, USA; ysu10@crimson.ua.edu (Y.S.); ekadanu@ua.edu (E.K.A.); steven.jones@ua.edu (S.J.)
[2] Transportation Policy Research Center, Alabama Transportation Institute, Tuscaloosa, AL 35401, USA
* Correspondence: zzhang124@ua.edu
† Deceased author.

Abstract

Cyclists are vulnerable road users, and factors associated with cyclist injury severity may vary across geographic contexts. This study compares a spatial statistical model, Geographically Weighted Logistic Regression (GWLR), with a spatial machine learning model, Geographically Weighted Neural Network (GWNN). Eight years of North Carolina motor vehicle–bicycle crash data (2015–2022), comprising 6373 crashes, were analyzed, with marginal effects used to compare spatially varying relationships between the two models. Results show that older cyclist age, higher vehicle speeds, intersection locations, multi-lane roadways, and dark conditions are associated with higher probabilities of evident or more severe injuries. Cyclists over 65 years showed mean marginal effects of 15.0% in GWLR and 5.7% in GWNN, indicating a strong association with injury severity. Vehicle speed, intersection location, and unlit dark conditions exhibit strong spatial heterogeneity, with elevated effects concentrated mainly in western and central North Carolina. GWNN achieved 73.7% accuracy on the test set, while GWLR achieved 64.7% accuracy on the full estimation sample. Despite different modeling frameworks, both models identified similar spatial patterns of local effects for most risk factors. These findings highlight the predictive capability of spatial machine learning while retaining interpretable geographic variation, supporting targeted bicycle safety interventions.

Keywords: cyclist injury severity; spatial heterogeneity; spatial machine learning; geographically weighted neural network; marginal effect

Academic Editor: Xiaobao Yang

Received: 13 August 2026
Revised: 14 September 2026
Accepted: 17 September 2026
Published: 19 September 2026

1. Introduction

Bicycling has resurged over the past decade for both transportation and recreation, particularly following the COVID-19 pandemic as people sought safer, socially distanced travel options [1,2]. However, cyclists are vulnerable road users and face a high risk of severe injury in motor vehicle crashes [3]. In the United States, more than 1000 cyclists are killed annually in traffic crashes, with tens of thousands more injured [3,4]. For example, 1166 pedalcyclist fatalities and approximately 49,989 pedalcyclists injured were reported in 2023 [5].

To address this issue, a substantial body of research has sought to identify the factors contributing to cyclist injuries in crashes [6–12]. These factors include roadway or infrastructure attributes, traffic conditions, motor vehicle features, driver and cyclist behaviors, manner of crash, and environmental characteristics [6–8,12–15]. Even though cycling and cyclist-involved crashes exhibit spatial variations, many studies do not explicitly account for this variation within the model structure, implicitly assuming that the effects of contributing factors are homogeneous across space. Ignoring such spatial non-stationarity can mask important local variations in risk relationships, leading to unobserved heterogeneity in model estimates [16] and limiting the effectiveness of generalized safety policies in addressing location-specific safety challenges [17–20]. To account for the spatial heterogeneity in factors related to crash injury severity, geographically weighted spatial regression and its variants (e.g., geographically weighted logistic regression, geographically weighted ordinal logistic regression, etc.) [8,21] are used to capture spatial variation by allowing the estimated coefficients to vary across space. However, these statistical models often need to satisfy strict prerequisite assumptions, hence have limited capacity to capture nonlinear relationships, and primarily focus on identifying associations rather than on prediction [22,23].

Due to their proficiency in modeling nonlinear relationships and prediction power, supervised machine learning (ML) methods coupled with interpretation techniques are increasingly being applied in predicting crash injury severity and identifying the relationship between risk factors and crash outcomes [24]. These approaches are particularly useful in situations where injury severity needs to be inferred for crashes with unknown outcomes or forecasted for crashes that may occur in the future [25]. However, these advantages should not be interpreted as implying that ML models are uniformly superior to traditional statistical approaches. Statistical models remain advantageous when parameter inference and direct interpretation of risk relationships are primary objectives, whereas many ML models require additional interpretation techniques to explain their predictions. Recent systematic reviews of ML-based crash modeling similarly emphasize that predictive performance must be considered together with issues such as interpretability, model evaluation, transferability, and robustness rather than accuracy alone [26–28]. In particular, Ali et al. [26] identify the integration and comparison of statistical and machine-learning approaches as an important direction because the two modeling paradigms provide complementary strengths in explanation and prediction. Incorporating ML models within a spatial modeling framework has emerged as a promising approach to leverage the predictive strength of ML while accounting for spatial heterogeneity [29–33]. For example, Gu et al. [30] developed a geographically weighted random forest (GRF) model to analyze crash frequency at intersections and found that GRF effectively addressed collinearity issues and demonstrated superior performance compared to the global random forest model. Similarly, Zhang et al. [29] proposed a Geographically Weighted Neural Network (GWNN) framework to model injury severity in speeding-related crashes, showing improved predictive accuracy and enhanced ability to capture spatially varying relationships compared to the global NN model. More recent spatial ML studies have likewise demonstrated the usefulness of geographically explicit ML frameworks for traffic-safety analysis [29,34,35].

However, the existing spatial ML literature has predominantly evaluated whether incorporating geographic weighting improves a corresponding global ML model. Such comparisons primarily establish improvements in prediction, model fitness, or locally varying feature importance, but do not directly address whether spatial ML and conventional spatial statistical models provide consistent geographical interpretations of the same safety relationships. This distinction is important because two models may differ not only in predictive performance but also in the direction, magnitude, and geographical distribution of estimated local effects, potentially leading to different conclusions regarding where safety interventions should be prioritized. Traditional geographically weighted models such as GWLR explicitly estimate and map local coefficients, whereas spatial ML models provide greater functional flexibility but require additional interpretation to translate predictions into comparable local effects. Furthermore, a direct comparison of these two modeling paradigms that evaluates both predictive performance and the spatial pattern of individual risk-factor effects remains limited in crash injury severity research. This distinction also clarifies how the present study extends our earlier GWNN work [29]. This study uses GWNN as a representative spatial machine learning method and directly compares it with GWLR, a representative spatial statistical model, in a common application scenario involving the severity of injuries among cyclists. Using marginal effects as a universal interpretability metric, this study not only compares the predictive performance of the models but also examines whether GWNN and GWLR can identify consistent spatial patterns in terms of the direction and magnitude of various influencing factors. Consequently, the study extends the traditional comparison between global machine learning and spatial machine learning to a comparison of spatial statistical models and spatial machine learning in terms of predictive capability and geographically explicit interpretability. Therefore, the methodological contribution of this study lies not only in the application of geographically weighted modeling methods, but also in establishing a common framework that allows spatial statistical models and spatial machine learning models to be directly compared using marginal effects on the same probability scale.

Considering the aforementioned research gaps, the objective of this study is to investigate spatial heterogeneity in factors influencing cyclist injury severity in traffic crashes by applying both traditional spatial statistical models and spatial machine learning models and systematically comparing their prediction performance and explanatory ability. Specifically, the following research questions are intended to be answered in this study:

RQ1—What factors are associated with cyclist injury severity in traffic crashes and to what extent do the effects of these factors vary across geographic space?

RQ2—How do spatial ML models compare with traditional spatial statistical models in predicting cyclist injury severity?

RQ3—Do spatial ML models and traditional spatial statistical models capture similar or different spatial patterns in the relationships between contributing factors and injury severity?

To address these research questions, this study develops a comparative analytical framework integrating the spatial statistical model and spatial machine learning model for crash severity modeling. Specifically, geographically weighted logistic regression (GWLR) is adopted as a representative spatial statistical model, and GWNN is employed as the spatial machine learning model. Using eight-year bicycle–motor vehicle crash data from North Carolina between 2015 and 2022, cyclist injury severity is modeled using both approaches to compare their prediction performance and examine their ability to capture spatial heterogeneity in risk relationships. Marginal effects are employed as a comparative interpretation tool to quantify the direction and magnitude of spatial variations identified by the GWLR and GWNN models. The outcomes of this study are expected to (1) provide a comparative framework for evaluating spatial statistical models and spatial machine learning models in terms of predictive performance and spatial interpretability; (2) advance understanding in spatial machine learning by empirically examining whether the additional flexibility of spatial machine learning produces similar or different spatial patterns compared with well-established spatial statistical models; and (3) offer insights for policymakers and practitioners to develop localized bicycle safety interventions.

This paper is organized as follows. Section 2 reviews the literature on factors related to cyclist injury severity and modeling methods. Section 3 presents the comparative framework. Section 4 describes the data. Sections 5 and 6 present modeling methods and modeling results. Section 7 discusses and compares the prediction performance and the spatial explanations revealed by GWLR and GWNN, as well as related localized safety interventions. Section 8 shows the limitations, and Section 9 concludes this study.

2. Literature Review

Recent studies have identified multiple factors that influence cyclist injury severity, including cyclist characteristics and behavior, driver attributes and behavior, collision configuration, roadway and traffic environments, and temporal factors [6,9,14,29]. For instance, vehicle operating speeds and high-speed roadways are consistently associated with more severe cyclist injuries [36–38]. Nighttime conditions, poor lighting, and adverse weather are also linked to increased injury severity [37,39]. Crash configurations such as overtaking, sideswipe, and angled collisions, particularly at intersections or access points, are more likely to result in severe injuries [7,40–42]. Roadway characteristics including multi-lane or wide road sections, which typically have higher speeds and more complex vehicle interactions, are also associated with greater injury [12,14,43]. Regarding cyclist and driver characteristics, older cyclists are more vulnerable to severe injuries, while crashes involving alcohol use are more likely to lead to serious or fatal outcomes [6,41,44]. A summary of key factors that influence injury severity in cyclist-involved crashes identified in prior studies is provided in Table 1. Methodologically, these factors may exhibit nonlinear relationships with injury severity, and their effects may vary across space due to unobserved spatial heterogeneity, motivating the use of modeling approaches capable of capturing both nonlinearities and spatial variation.

Table 1. Summary of selected studies and key findings related to cyclist injury severity.

Variable Category	Key Factor	Authors	Main Findings
Cyclist Attributes and Behaviors	Age, Gender, Helmet Use	Kim et al. [6]; Wahi et al. [45]; Chandia-Poblete et al. [46]	✓Older cyclists are more likely to sustain severe or fatal injuries due to higher physical vulnerability. ✓Male cyclists are overrepresented in severe-injury crashes, largely reflecting higher exposure. ✓Helmet non-use is associated with increased head injury severity. ✓Alcohol involvement by either cyclist or driver significantly increases the probability of severe injury.
Driver Attributes and Behaviors	Age, Impairment (e.g., alcohol, drug, etc.) Speeding/risk driving	Dozza [47]; Liu et al. [8,48]; Samerei et al. [49]; Dash et al. [9]; Lin et al. [50]; Scarano [41]	✓Crashes involving older or impaired drivers increase the likelihood of severe cyclist injury. ✓Speeding-related driver behavior significantly elevates injury severity risk.
Crash Configuration	Overtaking, Sideswipe, Angle Crashes	Moore et al. [7]; Chao et al. [51]; Scarano [41]; Hargrove [52]	✓Motorist overtaking and sideswipe crashes are more likely to result in severe cyclist injuries. ✓Angle crashes at intersections show higher injury severity compared to non-conflict crashes.
Crash Location	Intersection, Driveway, Non-intersection	Liu et al. [42]; Xiao et al. [13]; Liu et al. [8]	✓Intersection and driveway-related crashes present higher injury severity due to complex yielding and turning movements.

Table 1. *Cont.*

Variable Category	Key Factor	Authors	Main Findings
Roadway Characteristics	Number of Lanes, Speed Limit	Kim et al. [6]; Alluri et al. [11]; Raihan et al. [12]; Rahimi et al. [14]; Dash et al. [9]; Janstrup et al. [53]; Zhang et al. [29];	✓Multi-lane and wider roadways are associated with higher cyclist injury severity. ✓Higher posted speed limits substantially increase the probability of severe injuries.
Traffic & Speed Environment	Vehicle Speed	Hosseini et al. [15]; Scarano [41]	✓Higher vehicle operating speeds correlate with fatal and serious cyclist injuries.
Environmental Conditions	Lighting, Weather	Liu et al. [8]; Macioszek and Granà [37]; Dash et al. [9]; SafeTREC [39]	✓Darkness and unlit roadways significantly increase cyclist injury severity. ✓Adverse weather conditions further elevate severity risk through reduced visibility and control.
Temporal Factors	Time of Day, Season	Dozza [47]; Asgarzadeh et al. [54]; Dong et al. [10]; Yuan et al. [55]	✓Nighttime crashes are more likely to result in severe cyclist injuries. ✓Higher injury severity is often observed during peak cycling seasons.

To study factors associated with traffic crash injury severity, binary logit models, multinomial logit models, and ordered logistic regression have been extensively used [6,49,56,57]. These models typically assume a constant relationship between covariates and crash injury severity across observations and estimate a single global coefficient for each explanatory variable. To address unobserved heterogeneity from unmeasured factors, advanced logit models such as random parameter logit [17,58] and latent class logit models [59] have been widely used in crash injury severity analysis. Random parameter logit models allow coefficients to vary across observations, with interpretation based on the estimated mean parameters and variances that capture average effects and heterogeneity. In contrast, latent class models estimate a unique set of coefficients for each identified latent class. Considering crashes are inherently geo-referenced events, models capable of capturing spatial heterogeneity and supporting geo-localized interpretation can provide more safety insights by revealing how individual factors vary across space [17,60]. Geographically Weighted Logistic Regression (GWLR) and Geographically Weighted Ordinal Logistic Regression (GWOLR) extend traditional regression by estimating local logistic models and generating location-specific coefficients at each crash site, enabling the visualization of spatially varying relationships and supporting localized safety interventions [8]. However, because GWR is based on the logit model, nonlinear and interaction effects may not be fully captured, potentially leading to biased estimates in complex crash contexts [61,62]. In addition, as spatial statistical models are primarily designed for parameter estimation and spatial interpretation, GWR-based approaches do not emphasize out-of-sample predictive performance.

ML models have been increasingly adopted in transportation safety studies because of their ability to capture complex nonlinear relationships, accommodate interactions among predictors, and achieve strong predictive performance in out-of-sample settings [24,26,28]. Unlike traditional statistical models such as logistic regression and its variants, which are parametric and provide directly interpretable coefficients and statistical significance, many supervised ML models are often considered "black box" models due to their limited inherent interpretability [63]. Consequently, researchers frequently rely on post hoc interpretation techniques to explain model outputs without requiring access to the internal structure of the trained model. Among these approaches, feature importance measures are widely used to identify and rank influential predictors in crash severity modeling [64,65]. However, feature importance mainly provides a ranking of predictor contributions and does not indicate the direction or magnitude of their effects. To further interpret model outputs, methods such as marginal effects and partial dependence plots (PDPs) have been used to examine the relationships between predictors and predicted outcomes [44]. In addition, local explanation techniques, such as accumulated local effects (ALE) and Shapley additive explanations (SHAP), have gained increasing attention for interpreting individual predictions and revealing heterogeneous feature effects across observations [65–67]. When observations are geo-referenced, SHAP values can be visualized spatially to reveal geographically varying effects, an approach often referred to as GeoSHAP [62,68].

Recent studies have begun explicitly integrating machine learning algorithms with spatial modeling frameworks to develop spatially explicit machine learning approaches [29,30,32,33]. For example, Gu et al. [30] proposed a Geographical Random Forest (GRF) model to address multicollinearity among driving volatility indicators and used feature importance measures to examine spatial variations in predictor importance. However, this approach does not quantify the magnitude or direction of predictor effects on crash frequency. Zhang et al. [29] developed a GWNN framework that integrates neural networks with geographically weighted modeling to capture spatial variations in injury severity and its influencing factors. This approach improves predictive performance compared to an NN model and enables spatially explicit estimation of the magnitude and direction of the relationships between contributing factors and injury severity. However, existing spatial ML studies have primarily benchmarked geographically explicit ML models against their corresponding global ML counterparts [24,25,27,28]. These comparisons have mainly focused on improvements in prediction, model fit, or spatial variation in feature importance. They provide considerably less evidence on whether spatial ML and traditional geographically weighted statistical models identify consistent local relationships when applied to the same safety problem. In particular, direct comparisons of the direction, magnitude, and geographical distribution of predictor effects remain limited. Consequently, how spatial ML compares with traditional spatial statistical models in terms of both predictive performance and geographically explicit interpretation remains underexplored. In particular, direct comparison based on a common effect measure remains limited, making it difficult to determine whether the two modeling paradigms identify comparable directions, magnitudes, and spatial patterns of individual risk-factor effects.

In summary, two major gaps remain in existing literature. First, traditional spatial statistical models, such as GWLR, have been used to reveal spatial variations in cyclist crash risk factors, but they rely on predefined model structures and local linear assumptions, which may limit their ability to capture complex relationships between risk factors and cyclist injury severity in cyclist–vehicle crashes [8,17,60]. Second, although spatial machine learning approaches have recently been introduced, prior studies have mainly benchmarked them against global (non-spatial) machine learning models [29,30,32,33]. As a result, how spatial machine learning models compare with traditional spatial statistical models in terms of model performance and spatial interpretability remains underexplored.

3. Study Framework

This study proposes a comparative analytical framework (see Figure 1) for traditional spatial statistical modeling and spatial ML to investigate cyclist injury severity. The analysis is based on bicycle–motor vehicle crashes in North Carolina from 2015 to 2022. First,

https://doi.org/10.3390/futuretransp6050198

bicycle–motor vehicle crash data from North Carolina from 2015 to 2022 are cleaned, processed, and recoded, and explanatory variables are organized to represent cyclist and driver characteristics and behaviors, pre-crash factors, roadway and traffic characteristics, environmental and temporal conditions, and crash spatial context. Next, two spatial modeling approaches are developed and compared: GWNN, representing spatial machine learning, and GWLR, representing traditional spatial statistical modeling. A global NN model is also developed as a non-spatial benchmark. The global NN provides the base architecture for GWNN and serves as a reference for evaluating the additional predictive benefit obtained from geographic weighting. For the NN and GWNN models, the data are divided into training and testing sets, whereas GWLR is estimated using the full dataset in accordance with its primary role in local parameter estimation and spatial interpretation. Accordingly, predictive performance metrics from GWNN and GWLR are reported within their respective modeling frameworks rather than treated as strictly equivalent out-of-sample benchmarks. GWNN represents a machine-learning framework for which independent test-set evaluation is central to predictive assessment, whereas GWLR represents a spatial statistical framework primarily used for local coefficient estimation and spatial inference. Finally, marginal effects are used as a common interpretability measure across the models. Global marginal effects are calculated for the NN model, while local marginal effects are calculated for GWNN and GWLR. The two spatial models are then compared in terms of predictive performance and the direction, magnitude, and geographic distribution of their local effects to address the study's research questions.

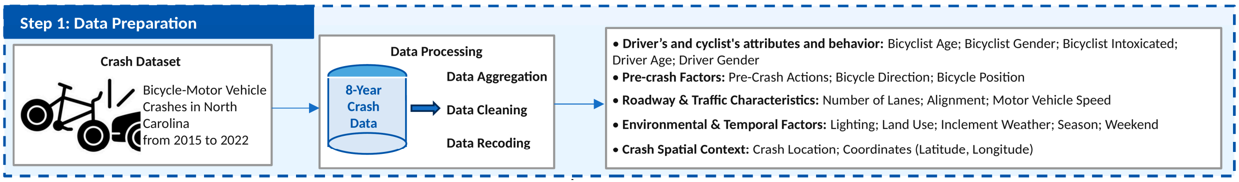

(**a**) Step 1—Data Preparation

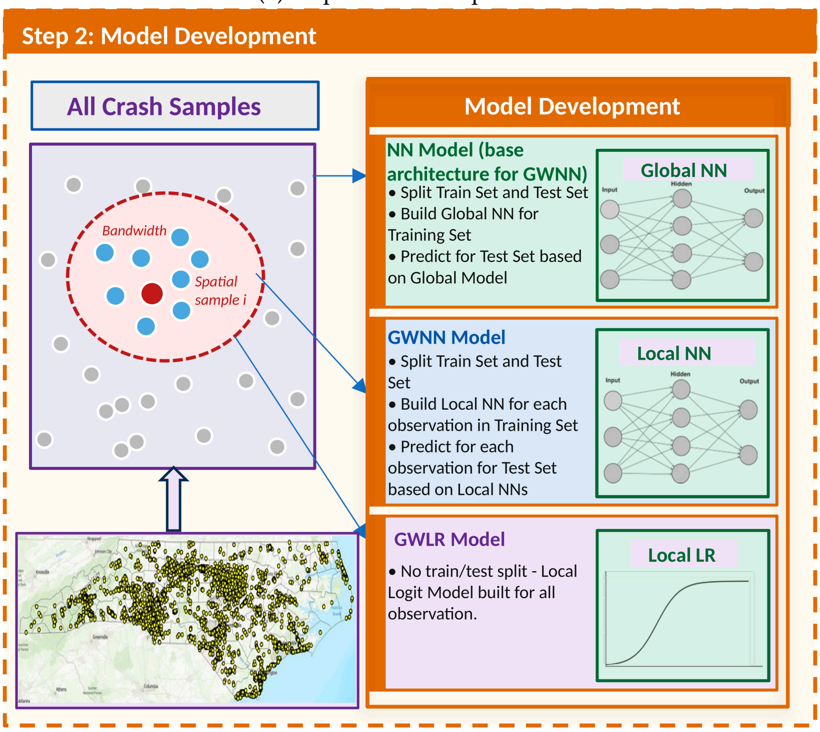

(**b**) Step 2—Model Development

Figure 1. *Cont.*

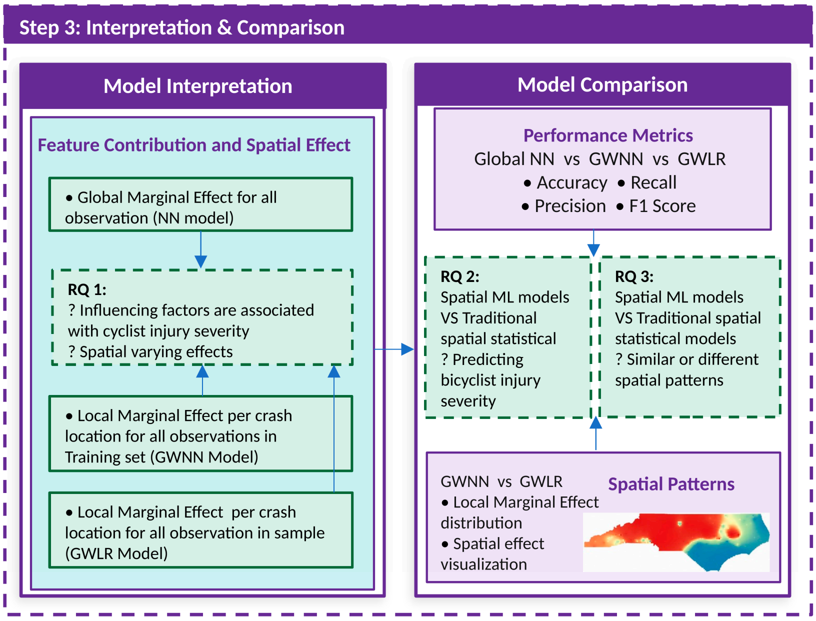

(**c**) Step 3—Interpretation & Comparison

Figure 1. Comparative analytical framework integrating spatial machine learning and spatial statistical modeling for cyclist injury severity.

4. Data

This study uses geo-referenced bicycle–motor vehicle crash data from the North Carolina Department of Transportation (NCDOT) from 2015 to 2022 [69]. Injury severity is coded according to the KABCO scale, where K stands for fatal injuries, A for suspected serious injury (traditionally termed an incapacitating injury), B for suspected minor injury, C for possible injuries, and O for no injuries [70]. The raw crash data were subjected to comprehensive error-checking and data processing procedures prior to modeling. Observations with missing values in key variables (e.g., cyclist injury severity and coordinates) or logically inconsistent values (e.g., implausible coordinates) were excluded from the analysis. Categorical variables were recoded for modeling purposes. The original five-level KABCO cyclist severity scale was recoded as a binary outcome distinguishing KAB from CO. According to the FHWA KABCO definitions, K, A, and B represent observable injury outcomes of increasing severity, whereas C represents a possible injury and O represents no apparent injury [70]. In addition, FHWA safety practice recognizes both KA- and KAB-based severity groupings for highway safety analysis and HSIP project selection [71]. This study uses KAB-based severity groupings because they align with the focus of this study and provide a more balanced distribution of injury severity outcomes. In addition, after regrouping, KAB crashes account for 53.5% of the dataset and CO crashes account for the remaining 46.5%, yielding a more balanced distribution of the outcome variable and enhancing the performance of the machine learning models. The five-level KABCO frequencies reported in Table 2 are presented for descriptive purposes only, to document the injury-severity distribution of the raw NCDOT records prior to regrouping. All subsequent modeling and predictive evaluation are conducted on the binary outcome. Binary indicators were subsequently constructed for all relevant categorical predictors for modeling purposes. After data preprocessing, a total of 6373 bicycle–motor vehicle crashes were retained in the final dataset for analysis.

Table 2. Descriptive statistics of model variables after data processing (N = 6373).

Variable		Frequency	Percent	Variable		Frequency	Percent
Cyclist Injury severity	O: No injury	651	10.2%	Pre-crash action	Cyclist failed to yield	1149	18.0%
	C: Possible injury	2313	36.3%		Cyclist overtaking	137	2.2%
	B: Suspected Minor Injury	2777	43.6%		Motorist failed to yield	1315	20.6%
	A: Suspected Serious Injury	454	7.1%		Motorist overtaking	1413	22.2%
	K: Killed	178	2.8%		Other	2359	37.0%
Cyclist age	≤10 yrs old	295	4.6%	Bicycle direction	Facing the traffic	1703	26.7%
	11–18 yrs old	1217	19.1%		With the traffic	4045	63.5%
	19–24 yrs old	846	13.3%		Other or unknown	625	9.8%
	25–36 yrs old	1077	16.9%	Crash location	Non-intersection	2835	44.5%
	37–51 yrs old	1179	18.5%		Intersection	2928	45.9%
	52–65 yrs old	1363	21.4%		Intersection-related	604	9.5%
	>65 yrs old	381	6.0%		Unknown	6	0.1%
	unknown	15	0.2%	Lighting	Daylight	4648	73.1%
Cyclist gender	Male	5335	83.7%		Dark—Lit Roadway	789	12.4%
	Female	1023	16.1%		Dark—Roadway Not Lit	609	9.6%
	Unknown	15	0.2%		Other	317	5.0%
Cyclist intoxicated (Yes)		265	4.2%	Land use	Urban (>70% Developed)	4510	70.8%
Bicycle position	Travel Lane	4003	62.8%		Mixed (30% to 70% Developed)	974	15.3%
	Bike Lane	432	6.8%		Rural (<30% Developed)	889	14.0%
	Sidewalk	1359	21.3%	Number of lanes	≤2 lanes	3660	57.4%
	Driveway	75	1.2%		3–4 lanes	1619	25.4%
	Other	504	7.9%		>4 lanes	920	14.4%
Driver age	≤19 yrs old	342	5.4%		Unknown	174	2.7%
	20–29 yrs old	1195	18.8%	Motor vehicle speed	≤15 mph	228	3.6%
	30–39 yrs old	1012	15.9%		16–25 mph	1117	17.5%
	40–49 yrs old	850	13.3%		26–45 mph	3927	61.6%
	50–69 yrs old	1498	23.5%		>45 mph	683	10.7%
	≥70 yrs old	533	9.0%		unknown	418	6.6%

Table 2. *Cont.*

Variable		Frequency	Percent	Variable		Frequency	Percent
	unknown	903	14.2%	Season	Spring	1511	23.7%
Driver gender	Male	3066	48.1%		Summer	1981	31.1%
	Female	2410	37.8%		Fall	1866	29.3%
	Unknown	903	14.2%		Winter	1015	15.9%
Driver intoxicated (Yes)		75	1.2%	Inclement weather (Yes)		312	4.9%
Weekend		1604	25.2%	Alignment (Curve)		334	5.2%

Figure 2a visualizes the geographic locations of all bicycle-related crashes, showing clear clustering in major urban areas with relatively larger populations and higher levels of bicycling activity, including Charlotte, the NC Triangle, Fayetteville, Wilmington, Asheville, and Greensboro. These areas span diverse geographic contexts, with Charlotte and the NC Triangle area representing large metropolitan regions, Asheville located in the mountainous western area, and Wilmington situated along the coast. Figure 2b,c further distinguish crashes by injury severity. Figure 2b shows the spatial density of crashes resulting in evident or more severe cyclist injuries, while Figure 2c presents the density of crashes involving possible or no injuries. Overall, the spatial pattern of severe injury crashes in Figure 2b largely mirrors the distribution of all crashes shown in Figure 2a, indicating that areas with higher crash exposure also experience higher counts of severe outcomes. However, a comparison between Figure 2b,c reveals notable spatial variation in bicycle crash injury severity across the study area. While Charlotte and the NC Triangle remain prominent hotspots across both severity categories, the concentration of severe injury crashes in cities such as Greensboro and Fayetteville is substantially weaker relative to their injury crash hotspots.

Table 2 summarizes the descriptive statistics of the variables used in the modeling. Most bicycle-motor vehicle crashes result in minor injuries, with suspected minor injuries accounting for 43.6% of cases and possible injuries accounting for 36.3%, whereas serious injuries account for 7.1% of cases and fatalities account for 2.8%. Younger cyclists aged 11–18 years represent 19.1% of crash victims, while the largest share involves cyclists aged 52–65 years, accounting for 21.4% of crashes. Males constitute the majority of cyclist victims, accounting for 83.7% of cases. Approximately 4.2% of injured cyclists were intoxicated, suggesting a potential risk factor for injury severity. Most crashes occur in travel lanes, which account for 62.8% of cases, indicating frequent interactions with motor vehicles, while sidewalks recorded 21.3% of crashes. Drivers aged 50–69 years are most frequently involved in bicycle crashes, accounting for 23.5% of cases, followed by those aged 20–29 years at 18.8%, and 1.2% of involved drivers were intoxicated, highlighting the role of impaired driving in cyclist safety. The most common pre-crash actions involve motorist behaviors, including overtaking cyclists in 22.2% of crashes and failing to yield in 20.6%, while cyclists failing to yield account for 18.0% of cases. At the time of the crash, 63.5% of cyclists were riding in traffic and 26.7% were traveling against traffic. Intersections account for 45.9% of crashes, and crashes occurring under dark conditions represent 22.0% of cases. Most crashes occur in urban areas, which account for 70.8% of cases, likely reflecting higher bicycling activity and traffic exposure. Roadways with speed limits of 26–45 mph account for 61.6% of crashes, while high-speed roads with speed limits above 45 mph account for 10.7%. Seasonally, crashes are most frequent in summer, accounting for 31.3% of cases, and fall, accounting for 29.3%, potentially reflecting increased bicycling activity during these periods.

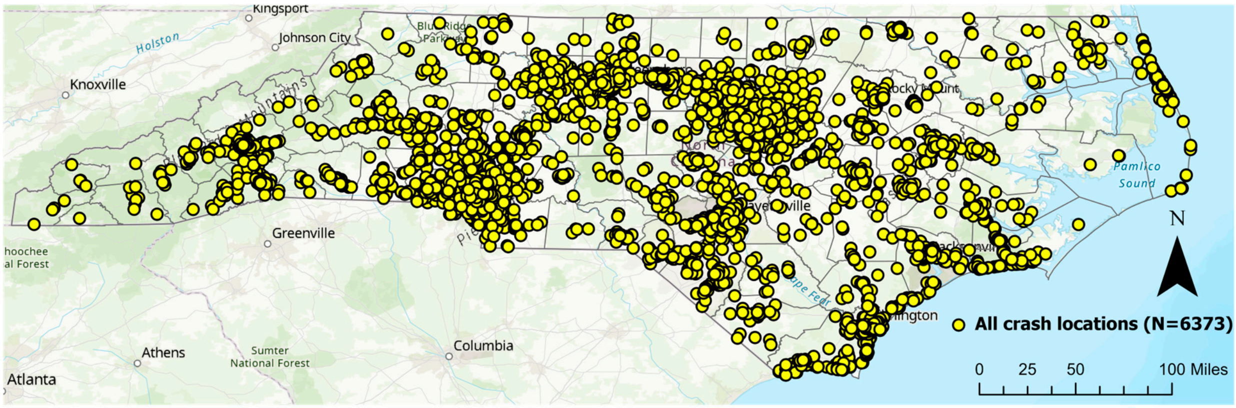

(**a**) All crash locations (N = 6373)

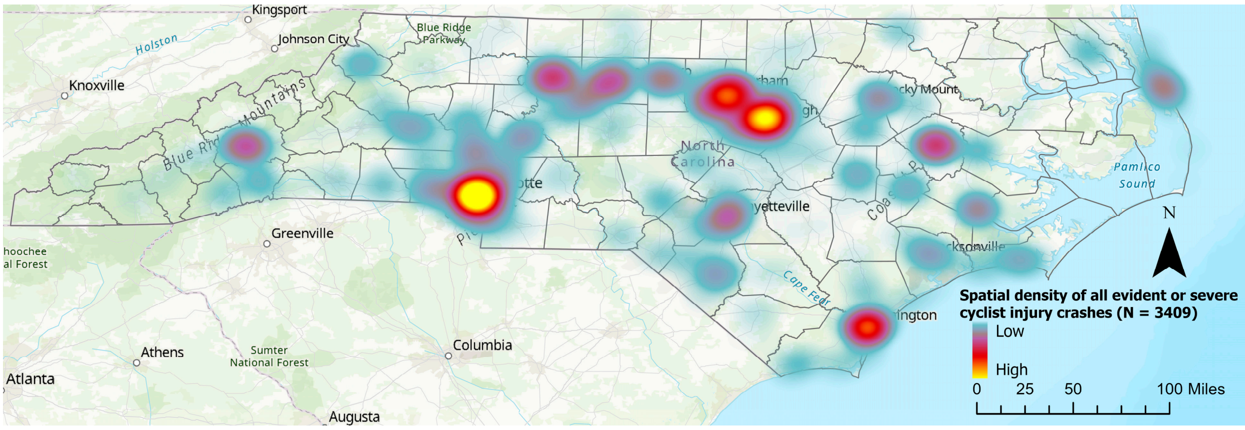

(**b**) Spatial density of all evident or severe cyclist injury crashes (N = 3409)

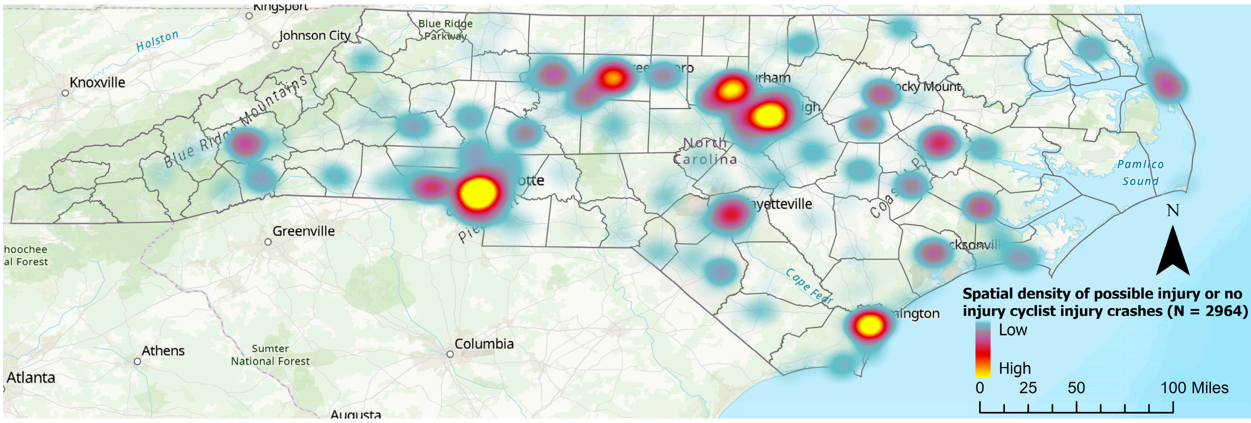

(**c**) Spatial density of possible injury or no injury cyclist injury crashes (N = 2964)

Figure 2. Spatial location and density of bicycle crashes in North Carolina from 2015–2022.

5. Methods

5.1. Neural Network

Neural networks (NN) are widely used machine learning methods that perform well in both regression and classification tasks [66,72–75]. An NN consists of an input layer, one or more hidden layers, and an output layer [76]. Numerous studies have demonstrated that NNs perform well in modeling crash injury severity and can effectively capture the non-linear relationships between risk factors and injury severity [77–80].

The full crash dataset was randomly split into 80% training and 20% testing sets using a fixed random seed to ensure reproducibility [29,81,82]. The 80/20 allocation was adopted as a conventional hold-out strategy that retains the majority of observations for model development while preserving an independent subset for out-of-sample evaluation. To determine the optimal NN architecture for crash classification, a hyperparameter tuning process was conducted using repeated random splits of the dataset combined with five-fold cross-validation. Key hyperparameters, including the number of hidden layers, neurons per layer, regularization strength, and dropout rate, were iteratively evaluated using validation accuracy and binary cross-entropy loss across folds. The final architecture includes an input layer followed by one hidden layer with 10 neurons with ReLU activation and L2 regularization to mitigate overfitting, and an output layer with a single neuron using a sigmoid activation function for binary classification. The model was trained with the Adam optimizer using an initial learning rate of 0.001 and binary cross-entropy loss. EarlyStopping was applied to terminate training when validation loss did not improve for ten consecutive epochs while restoring the best weights, and ReduceLROnPlateau reduced the learning rate by a factor of 0.1 after five epochs without improvement, with a minimum learning rate of 0.0001. Detailed hyperparameter settings are provided in Appendix A.1.

5.2. Marginal Effects

Marginal Effects (ME) are defined as the average predicted changes in the dependent variable resulting from a one-unit increase or a categorical change in a specific independent variable, while holding all other independent variables constant [40,83,84]. In this study, we calculate MEs using a function designed to work with a classification model trained in the Keras framework. In this study, all input variables are multi-class categorical variables. Before model training, these variables are converted into multiple binary indicator variables through one-hot encoding (dummy variable encoding), with each category corresponding to an independent dummy variable column. In the model input layer, the category features of each observation sample are represented by a set of mutually exclusive 0/1 encodings. This function predicts the average expected change in the dependent variable in response to variations in the independent variables. This study follows the partial dependence estimation framework, which has been widely applied in machine learning interpretability studies [20,63]. The model includes only categorical variables; no continuous variables are involved. Specifically, for a given categorical variable x_s, this study set all dummy variables to 0 to simulate the state of the variable in the reference category (baseline), while retaining the original observed values of all other variables x_c^i. The average predicted probability of the NN model output is $\hat{\mathrm{f}}_{\mathrm{Sbase}}$. Next, for each non-based class category in this variable, set the corresponding dummy variable to 1 (and 0 for the rest), keeping the other input variables unchanged, which is $\hat{f}_{Scategory}$. The difference ($\hat{\mathrm{f}}_{\mathrm{Scategory}} - \hat{\mathrm{f}}_{\mathrm{Sbase}}$) between the two is the average marginal effect for a specific category, as shown in Equation (1) [63,85]:

$$\text{Marginal Effects (ME)} = \hat{\mathrm{f}}_{\mathrm{Scategory}} - \hat{\mathrm{f}}_{\mathrm{Sbase}} \tag{1}$$

And the partial function is estimated by Equation (2):

$$\hat{\mathrm{f}}_{\mathrm{s}}(\mathrm{x}_{\mathrm{s}}) = \frac{1}{\mathrm{n}}\sum\nolimits_{1=1}^{\mathrm{n}} \hat{\mathrm{f}}\left(\mathrm{x}_{\mathrm{s}}, \mathrm{x}_{\mathrm{c}}^{\mathrm{i}}\right) \tag{2}$$

where $\hat{f}_s(x_s)$ is the average predicted output when feature x_s is set to a fixed category, and x_c^i represents all other feature values for observation i. For example, the variable "Pre-crash action" includes multiple behavior categories, such as "Cyclist failed to yield," "Cyclist overtaking," "Motorist failed to yield," etc. (Table 1). Assuming "Others" is selected as the reference category, the model sets all relevant dummy variables to 0 to predict the results under the reference category. Then, by setting "Cyclist failed to yield" to 1 (and all others to 0), the ME of this behavior category can be calculated, i.e., its average impact on the probability of a crash occurring relative to the reference category. This approach allows us to accurately quantify the influence of each independent variable on the dependent variable within the context of our classification model. MEs were used as the common effect measure for model comparison because GWLR provides conventional regression coefficients and associated inferential statistics, whereas NN-based models do not produce directly equivalent coefficients, odds ratios, or *p*-values. Expressing effects as changes in predicted probability therefore enables the direction and magnitude of individual risk-factor effects to be compared consistently across the statistical and machine-learning models.

5.3. Geographically Weighted Logistic Regression

The GWLR model is one of the most widely used spatial statistical modeling approaches for modeling binary crash injury severity outcomes. It allows regression coefficients to vary continuously across space by estimating a localized logistic model at each crash location. GWLR (as shown in Equation (3)) enables the identification of spatial heterogeneity of the risk factors:

$$\mathrm{Logit}(\mathrm{P}|\mathrm{Y_i} = 1) = \alpha(\mathrm{u_i}, \mathrm{v_i}) + \beta(\mathrm{u_i}, \mathrm{v_i})\mathrm{X_i} \tag{3}$$

where Y_i = 1 stands for the fatalities and severe injuries in cyclist crash, Y_i = 0 otherwise (e.g., possible injury or no injury crashes); $\alpha(u_i,\ v_i)$ stands for the intercept at geographic location $(u_i,\ v_i)$, $\beta(u_i,\ v_i)$ represents the spatially varying coefficients, and X_i stands for vector of independent variables for the i observation.

The selection of an appropriate bandwidth is critical in GWLR, as it reflects a trade-off between capturing localized spatial variation and maintaining model stability. A smaller bandwidth produces more localized parameter estimates, enabling the model to capture fine-scale spatial variation in cyclist crash injury outcomes, but it may also increase sensitivity to noise and the risk of overfitting. Detailed bandwidth sensitivity results are provided in Table A2 (Appendix A.3). Conversely, a larger bandwidth yields smoother coefficient surfaces and more stable estimates, although important local spatial heterogeneity may be obscured. To account for spatial heterogeneity in crash density, an adaptive bi-square kernel function was employed to calculate spatial weights. This adaptive specification allows the effective spatial extent of each local model to vary according to the surrounding density of observations, while maintaining a consistent number of neighbors for local calibration. Such an approach is particularly suitable for cyclist crash datasets, where crash locations are unevenly distributed across urban and suburban areas. The GWLR results consist of location-specific coefficient estimates that describe spatial variation in the relationships between risk factors and cyclist injury severity. Spatial statistical models such as GWLR are typically interpreted through location-specific estimated parameters, whereas spatial machine learning models such as GWNN do not produce directly comparable coefficients. As illustrated in the proposed comparative framework (Figure 1), ME was computed for each local LR, which enabled comparison between the spatial effect estimates derived from the spatial statistical and spatial ML models. The GWLR was implemented in the R statistical computing environment.

5.4. Geographically Weighted Neural Network

We adopted the GWNN model, which is an SML model developed by Zhang et al. [29]. Algorithm 1 presents the pseudo-algorithm and workflow of the GWNN model. The dataset was randomly split into training (80%) and testing (20%) subsets. During training, GWNN constructs a local NN for each observation in the training set using geographically weighted neighboring samples. The geographical distance used in GWNN is not treated as an explanatory variable directly affecting cyclist injury severity; rather, it serves as a localization mechanism inherited from the geographically weighted regression framework.

Following Tobler's First Law of Geography and the concept of spatial non-stationarity, observations closer to a target location are assumed to provide more locally relevant information for estimating the relationship between crash characteristics and injury severity [86]. This does not imply that distance itself influences injury severity. Instead, distance-based weighting allows the relationship between the explanatory variables and injury severity to vary across geographic space and can partially account for spatially structured contextual factors that are not fully represented by the observed covariates. Therefore, the weighting mechanism is theoretically motivated by the geographically weighted modeling framework rather than being introduced solely to improve predictive performance. After constructing all local models, the algorithm predicts crash outcomes for testing data based on the trained local NN model and evaluates performance using accuracy, recall, precision, and F1-score. The GWNN modeling procedure consists of the following main steps:

- Local observations and spatial weights.
  For each target observation, spatial weights are computed according to the geographic distances between that observation and all others, with the target location shifting sequentially through the dataset. This study adopts the commonly used bi-square kernel weighting (BKW) function, as shown in Equation (4):

$$\mathrm{w_j(u_i, v_i)} = \left(1 - \left(\frac{\mathrm{d_{ij}}}{\mathrm{d_{bandwidth}}}\right)^2\right)^2 \quad (4)$$

  where $w_j\ (u_i,\ v_i)$ stands for spatial weight for *ith* observation in the local sample for target observation, $(u_i,\ v_i)$ is the location of *ith* observation, d_{ij} is the geographical distance between *jth* observation and the target observation. $d_{bandwidth}$ stands for the geographic distance between the center of the subgroup and the farthest observation in the subgroup. The larger the bandwidth, the longer the runtime; therefore, selecting the optimal bandwidth is important. To maintain a consistent spatial weighting scale between GWLR and GWNN, the bandwidth of 2300 identified through the GWLR bandwidth-selection procedure was also adopted for GWNN. Using the same bandwidth reduces potential confounding from differences in spatial neighborhood size and provides a consistent basis for comparing the spatial effects identified by the two modeling approaches.
- Local NN model and explanation.
  Spatial weights are assigned to all observations in the local subset to reflect their relative influence on the severe cyclist injury outcome at a specific location. Observations located closer to the focal point receive higher weights in the loss function, indicating greater relevance for estimating the local relationship. The geographically weighted loss function defined in this study is shown in Equation (5):

$$\mathrm{E} = -\frac{1}{\mathrm{N}}\sum_{\mathrm{i=1}}^{\mathrm{N}} \mathrm{w_i(y_i \times \log(p(y_i)) + (1 - y_i) \times \log(1 - P(y_i)))} \quad (5)$$

  where $P(y_i)$ stands for the predicted probability that observation i belongs to the severer cyclist injury category, while the y_i represents the observed class label, taking the value of 1 for severer cyclist injury crashes and 0 is otherwise. The geographic weights of the observations in the subgroups (as shown in Equation (4)) are assigned to each observation in the subsampled dataset. The same architecture as the global NN model was also kept in the local NN model. In the training stage, we used two techniques to reduce the risk of overfitting in the training dataset. 20% of the training dataset was randomly selected as the validation set to avoid overfitting, and early stopping was then applied to reduce overfitting. If the model's performance on the validation set does not improve for 20 consecutive epochs, training is stopped early. This approach allows the model to be better trained and helps to avoid overfitting [29]. The two steps are repeated until each observation in the training set has its own local NN model. Finally, the spatial variability relationship can be demonstrated by the sign and absolute value of the local ME. A positive value of local ME indicates that the feature is associated with an increased probability of injury in a crash. In contrast, a negative local ME value means that there is an inverse relationship between them. After calculating the local ME values for each feature, raster maps are created to display the variation in the local relationships between risk factors and the probability of injury in bicycle crashes.

- Model Testing.
  The GWNN model predicts crash outcomes for out-of-sample observations by weighting the predictions of local NN models based on both their geographic proximity to the test observation and their predictive performance on their respective training subsets. The contribution of each candidate NN model from the training set is determined using a Bi-square kernel weighting scheme, which assigns higher weights to models associated with locations closer to the prediction site. These weights are further adjusted based on the accuracy of each local NN model to ensure that models with stronger predictive performance exert greater influence. To identify the optimal level of spatial smoothing, multiple iterations were conducted using different bandwidth values, each representing a different number of local NN models contributing to the prediction surface. Equation (6) shows how the local NN models are weighted for prediction.

$$\mathrm{w_j(u_i, v_i)} = \left(1 - \left(\frac{\mathrm{d_{ij}}}{\mathrm{d_{bandwidth}}}\right)^2\right)^2 \times \alpha_\mathrm{j} \quad (6)$$

where the $w_j\ (u_i,\ v_i)$ represents the weight assigned to the *jth* site-specific local NN model that falls within the bandwidth-defined neighborhood of the target location; the $(u_i,\ v_i)$ stands for the position of *ith* target observation in the test part; and the d_{ij} refers to the geographic separation between the target observation and the location at which the *jth* local model was trained. $d_{bandwidth}$ stands for the maximum distance from the target observation to any local model included within this neighborhood, thereby defining the extent of the subgroup. The parameter α_j captures the predictive accuracy of the *jth* local NN model and is incorporated to reflect model accuracy in the training process. As a preliminary step, the weights are normalized following Equation (7), and the normalized values are then used to combine the predictions of the local NN models.

$$\mathrm{w_j}'(\mathrm{u_i, v_i}) = \frac{\mathrm{w_j(u_i, v_i)}}{\sum \mathrm{w_j(u_i, v_i)}} \quad (7)$$

where the $\mathrm{w_j}'(\mathrm{u_i, v_i})$ stands for the weights after normalization. Accordingly, the prediction for the ith test observation is computed as shown in Equation (8):

$$\mathrm{P(y_i = 1)} = \Sigma \mathrm{w_j}'(\mathrm{u_i, v_i}) \times \mathrm{P}\left(\mathrm{y_j} = 1\right) \quad (8)$$

where the $P(y_i = 1)$ stands for the probability, estimated by the *jth* local NN model, that the cyclist in the target observation will experience an evident or severer injury.

Algorithm 1: Pseudo-algorithm of geographically weighted neural network (GWNN).

Algorithm 1 Geographically Weighted Neural Network (GWNN)

Input:
Data: Processed bicycle crash dataset from NCDOT
$\Omega N \times K$: Training set with N observations
$\Omega M \times K$: Testing set with M observations
K: Number of features

Initialize $i = 1, j = 1, k = 1$
Phase 1: Training
for $i = 1$ *to* N **do** ▷ Loop for each observation in training set
Calculate spatial weight w_i and select the subset
Train the *ith* local NN model and save it in Ω_{mtrain}
for $k = 1$ *to* K **do** ▷ Loop for each feature
Calculate the marginal effect M_{ik} for *kth* feature
end for
end for
Phase 2: Testing
for $j = 1$ *to* M **do** ▷ Loop for each observation in testing set
Calculate spatial weight w_j and select the subset
Make prediction for *jth* observation
Save prediction result
End for
Output:
Calculate accuracy, recall, precision, and F1 score

5.5. Model Evaluation

For the evaluation of the models, we use accuracy, precision, recall, and F1 scores to evaluate the performance of the models. These metrics are shown in Equations (9)–(12):

$$\text{Accuracy} = \frac{\text{TP} + \text{TN}}{\text{TP} + \text{FP} + \text{TN} + \text{FN}} \tag{9}$$

$$\text{Recall} = \frac{\text{TP}}{\text{TP} + \text{FN}} \tag{10}$$

$$\text{Precision} = \frac{\text{TP}}{\text{TP} + \text{FP}} \tag{11}$$

$$\text{F1} = \frac{2 \times \text{Precision} \times \text{Recall}}{\text{Precision} + \text{Recall}} \tag{12}$$

where "TP" stands for True Positive, "TN" means True Negative, "FP" means False Positive, and "FN" means False Negative. These performance metrics were reported for both the training and testing sets for the NN and GWNN models. For the GWLR model, no training–testing split was applied; therefore, the metrics were calculated and reported directly based on the observations used in model estimation. This evaluation strategy reflects the different estimation procedures and analytical purposes of spatial statistical and machine learning models. A similar approach was adopted by Li [62] when comparing a spatial statistical model with XGBoost, where model-fit statistics for the spatial statistical model were calculated using the full dataset, whereas XGBoost performance was evaluated using an independent test set after model training and cross-validation. Accordingly, the performance metrics reported here should be interpreted within the respective estimation

https://doi.org/10.3390/futuretransp6050198

frameworks of GWLR and GWNN [62]. In addition, the coefficient of variation (CV) (as shown in Equation (13)) is used to quantify the variability of local ME in GWLR and GWNN models:

$$\mathrm{CV} = \frac{\mathrm{S.D.}_{\mathrm{k}}}{\mathrm{mean}(\mathrm{ME}_{\mathrm{k}})} \tag{13}$$

where $S.D._k$ means the standard deviation of the ME for factor k, ME_k means the ME value based on the global NN model for factor k. CV is defined as the ratio of the standard deviation of the marginal effect to its mean value, reflecting the consistency of the influence of a variable in different spatial units. The higher the CV value, the greater the difference in the role of the variable in different regions, and the more significant the spatial heterogeneity.

6. Results

6.1. Neural Network Model

Table 3 presents the results of the ME calculated based on the global NN model and model performance. The model achieves an accuracy of 71.3% on the training set and 70.6% on the validation set. Its performance on the test set shows an accuracy of 70.9% and a recall of 72.0%. In this model, the positive outcome (Y = 1) is defined as a cyclist being fatally or otherwise injured. A positive ME indicates an increased probability of a cyclist being killed or injured. A larger absolute value of the ME reflects a stronger influence of the variable on bicycle crash outcomes. The ME results showed that age appears to play a significant role, with older cyclists, particularly those over 65 years old, showing the highest ME at 11.7%. Conversely, younger age groups, especially those aged 19–24, exhibit lower ME. Female cyclists have a higher ME at 2.3% compared to males. The position of the bicycle at the time of the crash significantly impacts injury severity. Cyclist injury severity occurring in bike lanes and sidewalks is associated with lower injury severity, with MEs of −4.3% and −4.5%, respectively, while driveways show a positive ME of 2.9% and are associated with higher injury severity. Drivers aged 30–39 years have the highest positive ME at 4.3%, indicating a higher risk of causing severe injuries. Female drivers, however, show a significant negative ME at −5.1%. Intoxicated drivers marginally increase injury severity with an ME of 1.05%, while crashes on curves are linked to reduced severity at −6.3%. Regarding pre-crash actions, cyclist injuries involving a motorist overtaking a cyclist have a positive ME of 2.2%. Additionally, cyclists traveling with traffic have a higher ME (6.1%). One possible explanation is that cyclists riding against traffic can see oncoming vehicles, allowing them to anticipate conflicts and take evasive action, which may reduce crash severity compared to situations where vehicles approach from behind. Poor lighting conditions, particularly on dark, unlit roadways, are associated with higher injury severity at a rate of 5.5%. Cyclist injury severity on roads with more than four lanes has a high positive ME of 6.5%. Seasonal variations show that cyclist injuries in summer have a higher ME of 4.1% compared to other seasons.

Table 3. Results for global NN model.

Variable	Category	ME (Y = 1)
Cyclist Age (Base: 10 yrs old or younger)	11–18 yrs old	−1.3%
	19–24 yrs old	−2.4%
	25–36 yrs old	−0.6%
	37–51 yrs old	3.5%
	52–65 yrs old	4.2%

Table 3. *Cont.*

Variable	Category	ME (Y = 1)
	>65 yrs old	11.7%
	Other	0.2%
Cyclist gender (base: Male)	Female	2.3%
	Unknown	−2.8%
Cyclist intoxicated	Yes	0.9%
	Unknown	6.0%
Bicycle position (Base: Travel Lane)	Bike Lane	−4.3%
	Sidewalk	−4.5%
	Driveway	2.9%
	Other	−1.1%
Driver age (Base: 19 yrs old or younger	20–29 yrs old	1.3%
	30–39 yrs old	4.3%
	40–49 yrs old	−3.2%
	50–69 yrs old	0.9%
	≥70 yrs old	−1.5%
	Unknown	1.8%
Driver gender (base: Male)	Female	−5.1%
	Unknown	0.3%
Vehicle Speed (Base: ≤15 mph)	16–25 mph	1.0%
	26–45 mph	4.3%
	>45 mph	8.6%
	Unknown	−1.8%
Pre-crash action (Base: Others)	Bicyclist overtaking motorist	−0.4%
	Bicyclist failed to yield	−8.1%
	Motorist overtaking bicyclist	2.2%
	Motorist failed to yield	−3.3%
Bicycle direction (Base: Facing the traffic)	With the traffic	6.1%
	Other or unknown	4.3%
Crash location (Base: Non-intersection)	Intersection	7.5%
	Intersection-Related	−3.4%
	Unknown	−10.4%
Lighting (Base: Daylight)	Dark—Lit Roadway	3.50%
	Dark—Roadway Not Lit	5.5%
	Other	−1.8%

Table 3. *Cont.*

Variable	Category	ME (Y = 1)
Land use (Base: Urban (>70% Developed))	Mixed (30% to 70% Developed)	3.4%
	Rural (<30% Developed)	2.2%
Lane number (Base: $\leq$2 lanes)	3–4 lanes	−2.7%
	>4 lanes	6.5%
	Unknown	−1.1%
Weather (Base: Inclement Weather)	Other	1.2%
Weekend (Base: yes)	Other	−4.3%
Time of year (Base: Spring)	Summer	4.1%
	Fall	−0.2%
	Winter	−4.1%
Driver intoxicated	Yes	1.1%
	Unknown	3.0%
Alignment (Base: Straight)	Curve	−6.3%
	Other	−1.1%
Training set	Train loss	50.20%
	Train accuracy	71.30%
	Validation Loss	57.00%
	Validation accuracy	70.60%
Test set	Accuracy	70.9%
	Recall	72.0%
	Precision	73.2%
	F1	72.6%

6.2. Geographically Weighted Logistic Regression Model

Table 4 presents the results of the GWLR model by summarizing the distributions of ME for all explanatory variables. For each variable category, the mean, standard deviation, coefficient of variation (CV), minimum, quartiles, median, and maximum values of the local ME are reported. Considering that the model estimation processes differ between spatial statistical modeling (i.e., GWLR) and ML models (i.e., NN and GWNN), and the outcome variable is binary, accuracy, recall, precision, and F1 score were reported for the full estimation sample for GWLR and for the independent test set for GWNN. These metrics characterize model performance within their respective frameworks and are not treated as directly equivalent measures of out-of-sample predictive performance [62]. The GWLR model achieved a whole-sample accuracy of 64.7%, recall of 57.1%, precision of 71.2%, and F1 score of 63.4%. Most variables exhibit substantial dispersion in MEs, with wide ranges between minimum and maximum values and large CVs.

Table 4. Results for local GWLR model.

Variable	Category	Mean	Std	CV	Min	25%	50%	75%	Max
Cyclist Age (Base: 10 yrs old or younger)	11–18 yrs old	−1.5%	4.9%	−3.2	−13.9%	−1.7%	2.6%	5.0%	15.9%
	19–24 yrs old	−1.5%	7.4%	−4.8	−10.1%	−8.3%	3.5%	7.3%	14.2%
	25–36 yrs old	−2.1%	5.1%	−2.4	−16.8%	−2.1%	3.2%	6.9%	13.4%
	37–51 yrs old	2.9%	4.7%	1.6	−17.4%	−1.2%	1.1%	6.0%	13.2%
	52–65 yrs old	2.5%	6.3%	2.5	−15.5%	0.3%	1.9%	6.4%	12.8%
	>65 yrs old	15.0%	13.1%	0.9	−1.6%	13.2%	15.7%	17.1%	33.3%
	Other	3.5%	8.4%	2.4	−9.7%	−5.3%	0.5%	13.8%	15.6%
Cyclist gender (base: Male)	Female	2.2%	7.1%	3.2	−2.9%	0.1%	2.9%	3.4%	13.9%
	Unknown	−8.7%	12.0%	−1.4	−29.6%	−10.5%	0.1%	0.9%	14.0%
Cyclist intoxicated	Yes	3.5%	7.2%	2.1	−10.5%	−1.1%	2.6%	8.1%	12.6%
	Unknown	1.9%	6.2%	3.3	−12.7%	−2.2%	2.9%	6.5%	11.2%
Bicycle position (Base: Travel Lane)	Bike Lane	−4.2%	6.2%	−1.5	−15.4%	−4.5%	0.1%	2.3%	18.6%
	Sidewalk	−3.9%	4.0%	−1.0	−13.0%	−6.7%	−5.2%	−2.9%	12.6%
	Driveway	2.8%	6.9%	2.5	−20.9%	−5.6%	6.6%	7.8%	31.4%
	Other	−2.2%	6.1%	−2.7	−18.1%	−7.3%	−0.8%	0.3%	8.9%
Driver age (Base: 19 yrs old or younger)	20–29 yrs old	0.9%	4.0%	4.5	−8.3%	−4.8%	−1.2%	6.2%	14.9%
	30–39 yrs old	3.2%	6.9%	2.2	−16.4%	−4.2%	4.9%	6.4%	10.7%
	40–49 yrs old	−2.9%	11.8%	−4.1	−26.7%	−11.0%	−6.2%	9.8%	20.8%
	50–69 yrs old	−3.4%	5.2%	−1.5	−31.6%	−6.3%	−2.0%	1.3%	9.0%
	≥70 yrs old	−4.3%	6.8%	−1.6	−34.1%	−7.8%	−6.0%	3.8%	10.7%
	Unknown	8.8%	12.2%	1.4	−34.5%	−0.3%	3.9%	18.9%	70.5%
Driver gender (base: Male)	Female	−2.2%	11.8%	−5.3	−9.6%	−5.7%	−3.6%	−1.6%	23.4%
	Unknown	2.1%	10.2%	5.0	−15.8%	−13.0%	3.8%	9.9%	20.5%
Vehicle Speed (Base: ≤15 mph)	16–25 mph	2.6%	10.0%	3.8	−10.9%	−4.9%	−0.2%	10.8%	25.1%
	26–45 mph	4.2%	10.4%	2.5	−10.3%	−2.0%	−0.3%	11.7%	23.2%
	>45 mph	13.1%	14.1%	1.1	−14.9%	3.8%	9.4%	27.2%	35.2%
	Unknown	1.8%	6.7%	3.7	−22.2%	−3.8%	1.1%	6.7%	32.4%
Pre-crash action (Pre-crash action (Base: Others)	Cyclist overtaking motorist	−3.4%	6.2%	−1.8	−9.8%	−5.6%	−1.7%	1.7%	10.6%
	Cyclists failed to yield	−8.2%	6.5%	−0.8	−19.4%	−11.7%	−8.2%	−7.5%	18.1%
	Motorist overtaking cyclist	0.4%	4.4%	11	−22.2%	−3.5%	−2.2%	−0.8%	6.4%
	Motorist failed to yield	−2.0%	5.8%	−2.9	−10.2%	−4.1%	−1.7%	0.5%	2.6%

Table 4. *Cont.*

Variable	Category	Mean	Std	CV	Min	25%	50%	75%	Max
Bicycle direction (Base: Facing the traffic)	With the traffic	4.3%	4.8%	1.1	−17.7%	4.2%	5.2%	8.4%	11.3%
	Other or unknown	4.9%	8.0%	1.6	−9.8%	−0.2%	6.6%	9.5%	14.0%
Crash location (Base: Non-intersection)	Intersection	1.3%	6.0%	4.5	−7.9%	−4.2%	−0.9%	1.0%	4.4%
	Intersection-Related	−3.9%	11.5%	−2.9	−14.9%	−10.2%	−2.2%	0.9%	13.0%
	Unknown	3.5%	10.9%	3.1	−13.8%	−9.9%	5.7%	8.9%	19.1%
Lighting (Base: Daylight)	Dark—Lit Roadway	3.1%	8.1%	2.7	−8.1%	−0.8%	2.1%	4.5%	20.7%
	Dark—Roadway Not Lit	10.6%	11.2%	1.1	−5.8%	−1.6%	11.4%	17.3%	22.1%
	Other	−1.3%	5.3%	−4.1	−16.9%	−3.7%	−1.4%	−0.1%	12.1%
Land use (Base: Urban (>70% Developed))	Mixed (30% To 70% Developed)	3.3%	8.2%	2.5	−7.6%	0.4%	2.6%	4.9%	16.0%
	Rural (<30% Developed)	2.5%	6.6%	2.6	−9.4%	−0.1%	3.0%	5.9%	11.9%
Lane number (Base: ≤2 lanes)	3–4 lanes	−0.6%	6.7%	−11.2	−12.6%	−3.5%	−1.9%	0.3%	3.6%
	>4 lanes	0.3%	7.8%	25.8	−11.4%	1.5%	2.9%	3.6%	12.1%
	Unknown	−7.6%	8.9%	−1.2	−15.9%	−10.9%	−9.6%	5.2%	16.8%
Weather (Base: Inclement weather)	Other	8.3%	5.1%	0.6	−3.4%	4.9%	6.7%	10.0%	14.9%
Weekend (Base: yes)	Other	−5.2%	4.0%	−0.8	−13.1%	−6.5%	−5.7%	−3.2%	1.6%
Time of year (Base: Spring)	Summer	1.5%	8.6%	5.6	−19.5%	−0.5%	1.6%	5.9%	12.5%
	Fall	1.5%	7.1%	4.7	−5.8%	−2.3%	0.4%	2.4%	29.3%
	Winter	1.4%	7.6%	5.5	−15.1%	−0.9%	1.2%	3.0%	11.1%
Driver intoxicated	Yes	0.5%	8.2%	16.2	−19.8%	−11.6%	−3.2%	5.5%	11.8%
	Unknown	−10.4%	10.8%	−1.0	−25.9%	−19.2%	−14.9%	−4.2%	10.9%
Alignment (Base: Straight)	Curve	−6.9%	10.0%	−1.4	−13.7%	−11.6%	−6.8%	−1.8%	2.7%
	Other	1.8%	5.8%	3.3	−11.7%	−8.5%	−0.7%	5.7%	25.5%
Model Performance:								Bandwidth	2300
								Accuracy	64.7%
								Recall	57.1%
								Precision	71.2%
								F1 Score	63.4%

Cyclist-related characteristics, including age, gender, intoxication status, bicycle position, and bicycle direction, show considerable variation in both magnitude and sign of MEs across locations. For instance, cyclists older than 65 years have a mean ME of 15.0%, with values ranging from −1.6% to 33.3%, while cyclists aged 25 to 36 years range from −16.8% to 13.4%. These wide ranges indicate substantial spatial heterogeneity in the estimated relationships. The MEs for female cyclists range from −2.9% to 13.9%, while cyclists traveling with traffic range from −17.7% to 11.3%. Cyclist intoxication also shows notable spatial variation, with MEs ranging from −10.5% to 12.6%. Driver characteristics, such as age, gender, and intoxication status, also demonstrate strong spatial variability. For example, drivers aged 30 to 39 years show MEs ranging from −16.4% to 10.7%, while drivers aged 40 to 49 years range from −26.7% to 20.8%. Female drivers exhibit MEs ranging from −9.6% to 23.4%. Roadway, traffic, and crash context variables exhibit similarly heterogeneous patterns. Vehicle speed categories show increasing mean MEs at higher speed levels. Compared with the base category (≤15 mph), lower speed ranges such as 16–25 mph and 26–45 mph exhibit relatively modest mean MEs of 2.6% and 4.2%, respectively. In contrast, speeds greater than 45 mph show a substantially higher mean ME of 13.1%, with values ranging from −14.9% to 35.2%. The ME for bicycle position in driveways ranges from −20.9% to 31.4%, and the ME for dark roadways without lighting ranges from −5.8% to 22.1%. Other variables also present wide spatial distributions. For example, mixed land use areas range from −7.6% to 16.0%, while rural areas range from −9.4% to 11.9%. Seasonal effects also vary spatially, with summer ranging from −19.5% to 12.5%.

6.3. Geographically Weighted Neural Network Model

Table 5 summarizes the local MEs and the training, validation, and test performance of the GWNN model. In terms of model performance, the average training accuracy of the GWNN model was 75.0%, with individual model accuracies ranging from 69.7% to 82.0%. For the validation dataset, the average accuracy was 72.2%, with a standard deviation of 3.8%. Accuracy ranged from 60.8% to 91.2%. The average validation loss was 19.1%, with a standard deviation of 2.8% and a CV of 0.1, indicating a relatively stable loss rate. Loss values ranged from 11.6% to 26.5%. On the test set, the model achieved an accuracy of 73.7% and a recall of 77.0%. The precision was 74.6%, and the F1 score was 75.8%, indicating that the model effectively balances precision and recall. The GWNN model's performance, with generally improved accuracy and balanced precision and recall metrics, demonstrates its robustness in capturing the complex spatial patterns in the data. The detailed confusion matrix is presented in Appendix A.2. To illustrate the variation in ME obtained from the GWNN model, the results are summarized using statistical measures including mean, standard deviation, CV, minimum, 25th percentile, 50th percentile, 75th percentile, and maximum of the local ME for each variable. The CV is used to gauge the degree of variation in the local MEs within the GWNN model [29]. The results indicate a high degree of variability in several variables, as shown by absolute CV values greater than 1. These variables include cyclist age, cyclist gender, bicycle position, vehicle speed, bicycle direction, lighting conditions, land use, the summer season, number of lanes, pre-crash location, and road alignment. Despite variations in ME magnitudes, certain variables consistently positively impacted the likelihood of a cyclist getting injured across the study area. These variables include cyclists over the age of 65, crash location at an intersection, vehicle speeds over 45 mph, and dark roadways without lighting.

Table 5. Results for local GWNN model.

Variable	Category	Mean	Std	CV	Min	25%	50%	75%	Max
Cyclist Age (Base: 10 yrs old or younger)	11–18 yrs old	−1.1%	3.6%	−3.3	−5.8%	−2.2%	−1.1%	2.2%	8.5%
	19–24 yrs old	−1.0%	3.7%	−1.6	−6.1%	−2.1%	−1.1%	1.8%	11.4%
	25–36 yrs old	−1.9%	3.5%	−1.8	−12.5%	−4.3%	−1.9%	2.5%	13.6%
	37–51 yrs old	4.1%	4.3%	1.0	−8.7%	1.2%	4.1%	7.3%	16.9%
	52–65 yrs old	4.6%	5.1%	1.1	−10.9%	−1.8%	4.6%	9.7%	19.9%
	>65 yrs old	5.7%	6.8%	1.2	−14.5%	1.1%	5.7%	10.2%	25.9%
	Other	2.1%	1.0%	0.5	−0.9%	−1.5%	2.1%	2.8%	15.4%
Cyclist gender (base: Male)	Female	3.2%	4.5%	1.4	−10.3%	−0.2%	3.2%	6.4%	16.7%
	Unknown	−3.4%	3.6%	−1.1	−14.3%	−5.9%	−3.4%	−1.0%	7.4%
Cyclist intoxicated	Yes	3.6%	3.2%	0.9	−11.2%	−2.2%	3.6%	7.2%	13.3%
	Unknown	0.7%	3.6%	5.4	−13.6%	−1.6%	0.7%	2.8%	16.7%
Bicycle position (Base: Travel Lane)	Bike Lane	−3.2%	3.6%	−1.1	−14.0%	−5.6%	−3.2%	−0.8%	7.5%
	Sidewalk	−1.5%	3.6%	−2.4	−16.7%	−3.7%	−1.5%	0.8%	8.6%
	Driveway	2.8%	3.4%	1.2	−12.9%	−1.6%	2.7%	8.5%	17.9%
	Other	−3.1%	3.3%	−1.0	−12.9%	−5.3%	−3.1%	0.9%	6.7%
Driver age (Base: 19 yrs old or younger	20–29 yrs old	3.1%	3.5%	1.1	−7.4%	0.8%	3.1%	5.5%	13.7%
	30–39 yrs old	0.6%	3.4%	6.0	−9.8%	−1.8%	0.6%	2.9%	19.9%
	40–49 yrs old	−2.4%	3.5%	−1.5	−12.8%	−4.7%	−2.4%	0.0%	8.0%
	50–69 yrs old	4.1%	3.1%	0.8	−5.4%	2.0%	4.1%	6.3%	10.6%
	≥70 yrs old	−2.2%	3.6%	−1.7	−15.0%	−4.6%	−2.7%	0.2%	8.6%
	Unknown	1.3%	3.5%	2.6	−9.1%	−1.1%	1.3%	3.6%	13.7%
Driver gender (base: Male)	Female	−0.67%	3.3%	−4.9	−10.5%	−2.8%	−0.7%	1.5%	9.1%
	Unknown	5.02%	3.5%	0.7	−5.4%	−2.7%	5.0%	7.4%	15.4%
Vehicle Speed (Base: ≤15 mph)	16–25 mph	4.36%	3.5%	−0.8	−6.2%	2.5%	4.4%	6.7%	15.9%
	26–45 mph	2.31%	3.1%	1.3	−7.0%	−0.2%	2.3%	4.4%	11.4%
	>45 mph	1.73%	3.7%	2.1	−0.8%	0.3%	1.7%	9.8%	15.9%
	Unknown	−4.13%	3.6%	−0.8	−14.9%	−6.5%	−4.1%	−1.7%	9.6%
Pre-crash action (Base: Others)	Cyclist overtaking motorist	−0.2%	3.8%	−16.4	−11.6%	−3.8%	−0.2%	3.3%	11.1%
	Cyclists failed to yield	−1.5%	3.5%	−2.4	−18.9%	−3.6%	−1.5%	−0.9%	10.3%
	Motorist overtaking cyclist	2.9%	3.5%	1.2	−12.5%	−1.4%	2.9%	7.2%	16.4%
	Motorist failed to yield	−2.4%	3.4%	−1.4	−12.5%	−4.7%	−2.4%	0.2%	7.6%

Table 5. *Cont.*

Variable	Category	Mean	Std	CV	Min	25%	50%	75%	Max
Bicycle direction (Base: Facing the traffic)	With the traffic	2.4%	3.5%	1.5	−13.0%	−1.9%	2.4%	6.5%	14.3%
	Other or unknown	3.5%	3.1%	0.9	−8.1%	−1.2%	3.5%	5.2%	9.6%
Crash location (Base: Non-intersection)	Intersection	0.3%	3.3%	9.9	−14.5%	−2.3%	0.3%	5.9%	14.7%
	Intersection-Related	−2.2%	3.6%	−1.7	−12.9%	−4.6%	−2.2%	0.3%	8.6%
	Unknown	1.5%	2.5%	1.65	−11.7%	−1.2%	1.5%	5.2%	11.6%
Lighting (Base: Daylight)	Dark—Lit Roadway	3.9%	3.8%	0.7	−14.3%	−1.4%	3.9%	7.2%	13.6%
	Dark—Roadway Not Lit	0.5%	3.6%	7.0	−16.2%	−1.9%	0.5%	8.6%	17.7%
	Other	−0.3%	3.7%	−11.1	−17.4%	−2.5%	−0.3%	1.9%	15.1%
Land use (Base: Urban (>70% Developed))	Mixed (30% to 70% Developed)	3.8%	3.4%	0.9	−4.7%	−1.5%	3.7%	6.8%	16.1%
	Rural (<30% Developed)	4.1%	3.4%	0.9	−6.8%	−1.5%	4.1%	7.6%	14.3%
Lane number (Base: ≤2 lanes)	3–4 lanes	−2.4%	3.3%	−1.4	−12.4%	−4.6%	−2.4%	−0.1%	7.6%
	>4 lanes	1.8%	5.6%	3.1	−2.9%	0.5%	1.8%	10.3%	16.6%
	Unknown	−3.1%	3.5%	−1.1	−13.5%	−5.5%	−3.1%	−0.8%	3.3%
Weather (Base: Inclement weather)	Other	4.2%	3.1%	0.7	−4.1%	2.2%	4.2%	6.2%	12.6%
Weekend (Base: yes)	Other	−2.4%	3.2%	−1.3	−12.1%	−4.6%	−2.4%	0.2%	7.3%
Time of year (Base: Spring)	Summer	2.8%	3.4%	1.3	−11.9%	−1.4%	2.7%	5.9%	14.2%
	Fall	−2.1%	3.3%	−1.6	−11.4%	−4.4%	−2.1%	0.2%	4.6%
	Winter	−0.4%	3.5%	−8.4	−16.1%	−2.7%	−0.4%	1.8%	3.2%
Driver intoxicated	Yes	3.5%	3.1%	0.9	−8.8%	−1.8%	3.5%	5.1%	6.9%
	Unknown	−1.1%	3.6%	−3.3	−10.7%	−2.6%	−1.1%	2.3%	9.2%
Alignment (Base: Straight)	Curve	−2.1%	3.1%	−1.5	−6.2%	−3.9%	−2.1%	5.1%	10.0%
	Other	3.8%	3.2%	0.9	−5.7%	−1.6%	3.8%	5.9%	13.3%

https://doi.org/10.3390/futuretransp6050198

Table 5. *Cont.*

Variable	Category	Mean	Std	CV	Min	25%	50%	75%	Max
Local model Performance	Local model training accuracy	75.0%	1.8%	0.1	69.7%	73.8%	75.0%	76.2%	82.0%
	Local model training loss	16.5%	1.7%	0.1	11.4%	15.3%	16.5%	17.6%	21.5%
	Local model validation accuracy	72.2%	3.8%	0.1	60.8%	69.6%	72.2%	74.7%	91.2%
	Local model validation loss	19.1%	2.8%	0.1	11.6%	17.4%	19.1%	20.7%	26.5%
Test Set Performance:								Bandwidth	2300
								Accuracy	73.7%
								Recall	77.0%
								Precision	74.6%
								F1 Score	75.8%

7. Discussion

The increasing application of spatial machine learning in transportation safety research has raised questions regarding its similarities and differences compared with traditional spatial statistical models commonly used in crash injury severity analysis [8,21]. Traditional geographically weighted regression (GWR) based approaches in safety modeling primarily focus on estimating spatially varying parameters to reveal spatial heterogeneity and support localized safety countermeasures, with less emphasis on predictive performance [18,19,87]. In contrast, many spatial machine learning models aim to improve predictive accuracy relative to global machine learning models but are often considered less spatially interpretable and therefore less frequently used to derive safety insights [29,30,32]. This study contributes to this discussion by systematically comparing spatial machine learning approaches with their spatial statistical modeling counterparts.

7.1. Model Comparison

In this study, three models, global NN, GWLR, and GWNN, were developed to predict cyclist injury severity and generate interpretable safety insights. Among them, GWNN achieved the highest prediction accuracy on the independent test set at 73.7%, outperforming the global NN, which reached 70.9%. This finding is consistent with previous studies showing that incorporating spatial structure into machine learning models can improve predictive performance [29,30,32,33]. In addition, GWNN achieved an out-of-sample accuracy of 73.7%, whereas GWLR yielded a whole-sample accuracy of 64.7%. Therefore, beyond the descriptive performance metrics, the primary direct comparison between GWNN and GWLR in this study is based on marginal effects, which provide a common scale for evaluating the direction, magnitude, and spatial variation in individual risk-factor relationships. This difference likely reflects the ability of GWNN to capture nonlinear relationships and interaction effects in cyclist injury severity outcomes. GWLR estimates locally weighted logistic regressions at each crash location and assumes locally linear relationships between predictors and the log-odds of injury severity. Such a structure may limit its ability to represent interaction effects and threshold behaviors commonly observed in crash data (e.g., the interaction between high vehicle speed and poor lighting conditions). In contrast, GWNN integrates NN structures within a geographically weighted framework, enabling the model to represent nonlinear relationships while accounting for spatial heterogeneity. These findings suggest that incorporating nonlinear function approximation within a geographically weighted framework can improve predictive performance compared with traditional geographically weighted regression models.

Regarding model interpretability, the MEs generated by the three models were compared. In general, except for some categories with unknown values, the signs of the mean MEs in the GWNN model are consistent with those from the NN model and the mean MEs from the GWLR model, as well as with findings reported in previous studies [8]. This consistency indicates that all three models capture broadly similar relationships between risk factors and cyclist injury severity. The significant risk factors identified by the GWNN model (i.e., ME greater than 3.0%) include cyclists aged 37–51 years, 52–65 years, and >65 years, each compared against the baseline group of cyclists under 10 years of age; cyclist intoxication, roadway in dark with lighting, mixed development areas, rural development areas, and driver intoxication. These variables capture most of the significant risk factors identified by the GWLR and NN models and reported in previous studies [6,8,88]. However, vehicle speed greater than 45 mph, relative to the baseline of 15 mph or below, shows a substantial contribution in both the GWLR and NN models and has been identified as an important risk factor in previous studies [64,84]. In the GWNN model, however, it exhibits a positive but relatively small ME of less than 2.0%. Further investigation shows that the ME of vehicle speed ranges from −0.8% to 15.9% in GWNN and from −14.9% to 35.2% in GWLR. The GWNN estimates are more consistent with prior safety research, which generally links higher impact speed to greater cyclist injury severity [6,38,89]. One possible explanation is that GWLR relies on a locally linear LR structure and may produce unstable local estimates when the underlying relationships involve nonlinearities and variable interaction effects [19,23]. By contrast, GWNN uses a local NN structure that is better able to capture these complex relationships, resulting in a more stable spatial range of ME. However, GWNN may also attenuate the contribution of some influential risk factors. A similar pattern is observed for dark roadway–not-lit conditions. The global NN indicates a positive injury risk effect, and the GWLR mean ME is also strongly positive with a low CV, suggesting relatively small spatial variation. In contrast, GWNN produces a near-zero mean ME with a substantially higher CV, indicating stronger spatial variation. This result suggests that the effect of poor lighting may not be uniformly positive across space but might instead be moderated by local conditions such as speed and roadway infrastructure.

7.2. Spatial Variation

This section visualizes and discusses spatial variation in the local MEs generated by GWNN and GWLR for selected variables. The local MEs vary spatially in direction and magnitude, exhibiting consistently positive, consistently negative, or sign-changing patterns across North Carolina, depending on the variable examined. The selected variables include speed greater than 45 mph, light conditions (dark roadway–not lit), crash location (intersection), and cyclists over 65 years old. Figure 3 shows these spatial variations by using QGIS interpolation, specifically creating an Inverse Distance Weighting (IDW) surface for the variable MEs. The map colors indicate injury severity risk, with red and orange representing increased risk of severe outcomes and blue and green indicating decreased risk.

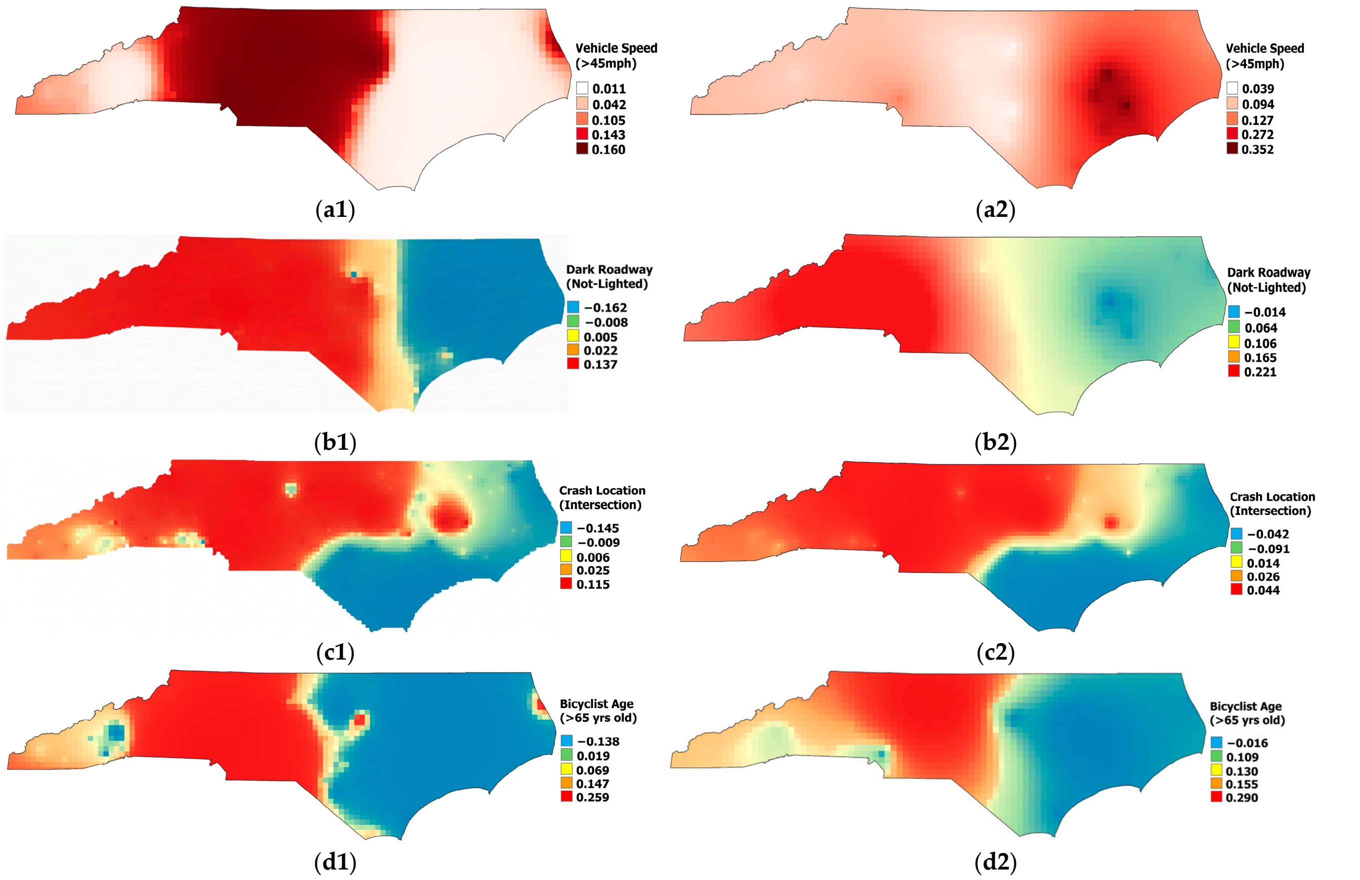

Figure 3. Spatial variation in local MEs based on GWNN (**a1**–**d1**) and GWLR (**a2**–**d2**) for selected variables. (**a1**) Vehicle speed >45 mph vs. ≤15 mph in GWNN model; (**a2**) vehicle speed >45 mph vs. ≤15 mph in GWLR model; (**b1**) dark roadway-not lit vs. daylight in GWNN model; (**b2**) dark roadway-not lit vs. daylight in GWLR model; (**c1**) Crash location—intersection vs. non-intersection in GWNN model; (**c2**) Crash location—intersection vs. non-intersection in GWLR model; (**d1**) cyclist age—>65 yrs old vs. 10 yrs old or younger in GWNN model; (**d2**) cyclist age—>65 yrs old vs. 10 yrs old or younger in GWLR model.

Figure 3(a1,a2) show the spatial distributions for vehicle speed above 45 mph. Both the GWNN (Figure 3(a1)) and GWLR (Figure 3(a2)) maps show positive local MEs for vehicle speeds exceeding 45 mph across North Carolina, echoing prior literature consistently linking higher motor-vehicle speeds to increased cyclist injury severity [6,90]. However, the spatial distribution of high MEs differs between the GWLR and GWNN models. The GWLR map reveals a west-to-east gradient, with relatively lower MEs in the Asheville region and peak values in the east-central and coastal corridor. The GWNN map exhibits a similar all-positive pattern, with peak MEs concentrated in the central-north corridor from Greensboro to the Triangle Area, whereas lower values are observed in the far west and along the southeastern coast. Empirically, the elevated risk in the central-north corridor identified by GWNN corresponds to high-volume, mixed-speed arterial networks around major urban centers where cyclists share road space with fast-moving traffic and is more consistent with the severe crash heat map. From an implementation perspective, the positive local effects of high vehicle speed can be used to identify priority corridors for speed-management assessment, particularly in the central and central-north areas highlighted by the GWNN results. Transportation agencies could first overlay these high-effect areas with severe-crash history, bicycle activity, posted and operating speeds, and existing bicycle facilities to identify specific corridors for field review. On identified corridors, countermeasures may include context-sensitive speed-limit review combined with engineering treatments that reduce operating speeds, such as road diets, lane narrowing, speed-feedback signs, and other traffic-calming measures. Where traffic speeds and volumes remain high, buffered or physically separated bicycle facilities should also be considered to reduce cyclist exposure to fast-moving vehicles [91–97].

Figure 3(b1,b2) visualize the spatial distribution of local MEs for the variable dark roadway, not lit. The two maps show similar spatial patterns in the western and central regions but diverge in the eastern region. The GWLR map (Figure 3(b2)) shows a predominantly positive west-to-east gradient: western North Carolina carries the highest local MEs, which diminish steadily toward near-zero or marginally negative values in the east. The GWNN map (Figure 3(b1)) exhibits a sharper spatial split: western and central regions remain positive, while eastern North Carolina reverses to negative MEs, suggesting that in the east, unlit dark conditions may not elevate and may even alleviate injury severity. The local ME from GWLR is larger than that from GWNN, while the higher CV in GWNN indicates stronger geographic differentiation. This might be explained from a model-structure perspective, as GWLR, being a locally linear model, tends to smooth nonlinear interactions among lighting conditions, road infrastructure, and the traffic environment, whereas the local NN may capture the same complex relationships among these factors [62]. Despite this divergence in the east, both models consistently identify western North Carolina as the high-risk region, where poor visibility compounds the effects of high vehicle speeds and limited road infrastructure on rural corridors. This echoes prior evidence that dark, unlit conditions amplify cyclist injury severity [8,98]. Accordingly, western and parts of central North Carolina identified by the local ME maps can be prioritized for nighttime visibility assessments. Agencies could first identify high-effect areas that also have a history of nighttime cyclist crashes or substantial nighttime bicycle activity. For these areas, continuous roadway lighting may be considered where nighttime risk extends along a roadway segment, while targeted lighting can be installed at intersections, crossings, curves, and other conflict locations. Complementary visibility treatments, including retroreflective pavement markings, enhanced delineation, and other conspicuity improvements, may also be considered where full roadway lighting is not feasible [99–104].

Figure 3(c1,c2) show the spatial distribution of local MEs for intersection crash locations. Intersections have been widely documented as high-risk locations due to complex right-of-way conflicts and multi-directional vehicle movements [7,40]. Both the GWNN and GWLR maps exhibit broadly consistent spatial patterns for crash location (intersections), while GWNN (Figure 3(c1)) captures a markedly wider range of spatial variation than GWLR (Figure 3(c2)). Both maps show the elevated injury severity across western and central-north North Carolina, while the southeastern and coastal regions reverse to negative MEs, suggesting that crashes that occur at intersections in those areas are associated with comparatively lower injury severity. Positive MEs concentrated in western and central-north North Carolina indicate that intersections in these areas should receive greater attention in bicycle-safety planning and project prioritization. Transportation agencies could combine the local ME patterns with severe-crash history, bicycle exposure, traffic volume, intersection geometry, and existing bicycle facilities to screen and prioritize candidate intersections for further safety assessment. At locations identified as high priority, engineering treatments may include protected bicycle crossings, dedicated or separated bicycle signal phases, improved sight distance, enhanced pavement markings, and other measures that reduce turning and crossing conflicts [105–107]. At the policy and programming level, these spatial results could also be incorporated into NCDOT and local Complete Streets planning and safety-improvement processes so that intersections exhibiting both elevated cyclist injury risk and deficient bicycle accommodation receive higher priority for multimodal investment. This type of risk-based prioritization is consistent with FHWA's systemic safety approach, which recommends identifying risk factors, screening and prioritizing candidate locations, selecting appropriate countermeasures, and then prioritizing projects for implementation [107–109].

Figure 3(d1,d2) illustrate the spatial distribution of local MEs for cyclists aged 65 and older. The GWLR and GWNN models exhibit similar spatial patterns, with positive local MEs covering the majority of the study area and concentrated in central NC, spanning the Charlotte–Greensboro and Triangle corridors, and transitioning to near-zero or negative MEs in eastern North Carolina. These patterns indicate that older cyclist age is more strongly associated with evident or severe injury outcomes in the central North Carolina corridor. This spatial variation is consistent with previous evidence regarding the greater physical vulnerability of older cyclists and the importance of age-sensitive cycling environments [88,95]. From a policy perspective, the spatial concentration of elevated age-related injury effects provides a basis for identifying corridors where age-sensitive bicycle safety interventions may be most needed. NCDOT and local transportation agencies could incorporate these spatial risk patterns into Complete Streets planning, bicycle and pedestrian project development, and systemic safety screening by combining them with information on older-adult populations, bicycle activity, traffic volumes, operating speeds, intersection complexity, and existing bicycle facilities [107–110]. Regions where stronger age-related injury effects coincide with high traffic stress or limited bicycle accommodation could be prioritized for infrastructure investment. Consistent with the Safe System approach, treatments in these locations may include physically separated bicycle facilities, lower-speed street design, protected intersections, reduced-conflict crossings, and other design features that reduce cyclists' exposure to high-energy vehicle conflicts [88,95,97,103,105,107–110]. Education and training programs tailored to older cyclists may also complement these engineering measures.

Overall, GWNN achieved 73.7% accuracy on the independent test set, compared with 64.7% for GWLR on the full estimation sample. Despite differences in model structure, the two models identify similar geographic patterns in the direction and spatial distribution of most risk factors, suggesting consistent identification of key safety factors. However, the magnitude of the local spatial effect differs between the two approaches. For some variables, the spatial patterns produced by GWNN align more closely with established safety knowledge, likely reflecting its ability to capture nonlinear and interactive relationships that are not represented in GWLR. From a broader perspective, these spatial results are intended to support screening and prioritization of locations for further safety assessment. The local ME maps do not prescribe a single countermeasure for all locations within a high-effect region. Transportation agencies can use the local ME maps to identify areas where a particular risk factor has a stronger association with cyclist injury severity and then combine this information with site-level crash history, bicycle exposure, roadway geometry, traffic conditions, and existing facilities to select candidate corridors for detailed engineering assessment. In North Carolina, these priority regions could be further evaluated within NCDOT's existing Complete Streets and bicycle/pedestrian project-development processes, which provide mechanisms for selecting bicycle facilities and multimodal improvements based on roadway context and user needs [108]. The final countermeasure could therefore be determined at the corridor or site level based on the identified risk factor and local roadway conditions.

8. Limitations

The findings of this study heavily rely on the quality of the bicycle crash data. One major issue is the lack of completeness in the data. For instance, whether a cyclist wears a helmet is a significant factor influencing cyclist injury severity, as has been documented in previous studies, yet this information was not included in our dataset. The absence of such key variables may result in models that fail to capture all potential risk factors, thus affecting the accuracy and interpretability of the results. In addition, this study adopted the KAB–CO binary injury severity grouping throughout the analysis, and sensitivity analyses using alternative severity groupings were not conducted. The selection of severity thresholds may affect the estimated relationships and model performance. This study is based on an empirical comparison of the predictive performance and explanatory capability of a spatial machine learning model and a geographically weighted statistical model using real-world motor vehicle–bicycle crash data. As such, the findings are data-driven and context-specific. Future research could incorporate controlled numerical experiments to further examine model behavior. Additionally, the GWNN model represents only one type of spatial machine learning approach. The results may vary when compared with other machine learning models.

9. Conclusions

This study compares a spatial machine learning model, the Geographically Weighted Neural Network (GWNN), with a traditional spatial statistical model, Geographically Weighted Logistic Regression (GWLR), for modeling cyclist injury severity. Using cyclist-vehicle crash data from North Carolina (2015–2022), a global NN was first developed to provide the base architecture for the GWNN, while GWNN and GWLR were used as the two principal spatial modeling approaches. Among the machine learning models evaluated on the independent test set, GWNN achieved the highest accuracy at 73.7%, compared with 70.9% for the global NN. GWLR achieved a whole-sample classification accuracy of 64.7% based on the full estimation sample. The GWNN's test set accuracy was therefore 9.0% higher than the GWLR's whole-sample accuracy, although the two values were obtained under different evaluation frameworks. Marginal effects (MEs) were used to quantify the direction and magnitude of contributing factors, and the mean MEs from the GWNN are generally consistent with those from the global NN and GWLR models. The analysis identifies several key factors associated with higher cyclist injury severity, including cyclist age over 65 years, which shows the largest contribution with mean MEs of 11.7% in the global NN and 15.0% in the GWLR model, followed by vehicle speeds greater than 45 mph and dark roadways without lighting. Intersections, roadways with more than four lanes, riding with traffic, mixed land-use environments, and the summer season also contribute positively to injury severity, though with comparatively moderate effects.

Spatial visualization of local MEs shows that GWLR and GWNN reveal similar geographic patterns in the direction and spatial distribution of most risk factors. Both models capture comparable spatial heterogeneity by identifying three distinct types of spatial feature variations in risk factors: consistent positive associations, consistent negative associations, and inverse associations, where MEs vary between positive and negative depending on location. Specifically, vehicle speeds greater than 45 mph exhibit consistently positive local MEs across the entire state in both models, whereas factors such as riding on sidewalks and curved roadway alignments show predominantly negative associations. In contrast, unlit dark roadway conditions, intersection locations, and cyclist age over 65 years display sign-changing patterns, with positive MEs concentrated in western and central North Carolina and near-zero or negative values in the eastern and coastal regions. However, the magnitude of the local spatial effects differs between the two approaches, with GWNN attenuating the influence of several factors and producing estimates that appear more consistent with established safety knowledge.

This study contributes both methodologically and empirically. Methodologically, it provides a systematic comparison between the GWNN and GWLR in terms of predictive performance and spatial interpretability for crash injury severity modeling. The findings provide additional confidence in applying spatially explicit machine learning approaches in traffic safety analysis and help bridge perspectives between researchers who favor traditional spatial statistical models, due to their clear model structure and coefficient estimation, and those exploring spatial machine learning approaches, which offer fewer modeling constraints, strong out-of-sample predictive capability, and the ability to capture nonlinear and interaction effects. These insights support the broader use of spatial machine learning for modeling geo-referenced safety events, such as crash frequency, injury severity, and hard braking events. Practically, this study identifies regions where specific risk factors are more likely to contribute to cyclist–vehicle crashes resulting in fatalities or injuries, providing guidance for localized safety interventions. For example, western and central North Carolina consistently emerge as higher-severity areas, driven by the combined influence of higher vehicle speeds and inadequate roadway lighting. These spatial findings can help prioritize regions for further engineering assessment. In areas where high vehicle speed has a stronger local effect, priority treatments may include context-sensitive speed management, traffic-calming or road-diet treatments, and greater separation between cyclists and motor vehicles. In areas where unlit nighttime conditions exhibit stronger effects, targeted or continuous roadway lighting and enhanced retroreflective delineation may be considered. Future research should (1) further compare spatial machine learning models (e.g., geographically weighted XGBoost, geographically weighted Random Forest) with their spatial statistical counterparts, (2) extend the proposed comparison framework using various interoperable methods to better understand their relative strengths and limitations in modeling geo-referenced traffic safety events, and (3) evaluate alternative binary or ordinal severity classifications to examine the robustness of the identified risk factors and spatial patterns across different injury severity definitions.

Author Contributions: Conceptualization, Y.S., Z.Z. and J.L.; methodology, Y.S., Z.Z. and J.L.; software, Y.S.; validation, Y.S. and Z.Z.; formal analysis, Y.S. and Z.Z.; data curation, Y.S.; writing—original draft preparation, Y.S., Z.Z., J.L.; writing—review and editing, Y.S., J.L., E.K.A., S.J. and Z.Z.; visualization, Y.S.; supervision, S.J. Author J.L. passed away prior to the publication of this manuscript. All other authors have read and agreed to the published version of the manuscript.

Funding: This research received no external funding.

Institutional Review Board Statement: Not applicable.

Informed Consent Statement: Not applicable.

Data Availability Statement: The data presented in this study are available from the corresponding author upon reasonable request.

Acknowledgments: The authors appreciate the data provided by the North Carolina Department of Transportation and the team of the North Carolina Pedestrian and Bicycle Crash Data Tool, who pre-processed and released the data for research. The authors received support from the Alabama Transportation Institute at the University of Alabama. ChatGPT-5.6 was used solely for editing and grammar-checking in the preparation of this manuscript. The views expressed in this paper are those of the authors, who are responsible for the factual accuracy of the information presented.

Conflicts of Interest: The authors declare no conflicts of interest.

Abbreviations

The following abbreviations are used in this manuscript:

GWR	Geographically weighted regression
SML	Spatial machine learning

GWNN	Geographically weighted neural network
GWLR	Geographically weighted logistic regression
MEs	Marginal effects
ML	Machine learning
GRF	Geographically weighted random forest
GWOLR	Geographically weighted ordinal logistic regression
NN	Neural network
PDPs	Partial dependence plots
ALE	Accumulated local effects
SHAP	Shapley additive explanations
NCDOT	North Carolina Department of Transportation
CV	Coefficient of variation
IDW	Inverse Distance Weighting

Appendix A

Appendix A.1

Appendix A.1 summarizes the hyperparameter settings used to configure and train the GWNN model. The model employed an adaptive bi-square kernel with a bandwidth of 2300 observations and an 80%/20% training–testing split. The neural network consisted of 44 input features, one hidden layer with 10 neurons using the ReLU activation function, and a single sigmoid output neuron for binary classification. Adam optimization and binary cross-entropy loss were used, with L2 regularization set to 0.0001. Training was limited to 40 epochs, with early stopping based on a patience of 20 epochs and a minimum improvement threshold of 0.001.

Table A1. Hyperparameter settings for the GWNN model.

Category	Hyperparameter	Value
Spatial Model	Bandwidth (k)	2300
	Kernel function	Adaptive bi-square
Data Split	Train/test split	80%/20%
Neural Network Architecture	Input dimension	44 features
	Neurons in hidden layer	10
	Activation function	ReLU
	Output layer	1 neuron
	Output activation	Sigmoid
Regularization	L2 regularization	0.0001
Optimizer	Optimization algorithm	Adam
Loss Function	Loss function	Binary cross-entropy
Training Configuration	Maximum epochs	40
	Early stopping patience	20
	Early stopping—min delta	0.001

Appendix A.2

Appendix A.2 (See Figure A1) presents the confusion matrix for the GWNN model based on the binary cyclist injury severity classification. Among the CO crashes, 414 were correctly classified as CO, while 179 were misclassified as KAB. For the KAB crashes, 525 were correctly classified as KAB and 157 were misclassified as CO. Overall, the matrix indicates that the GWNN model achieved relatively balanced classification performance across the two injury severity groups.

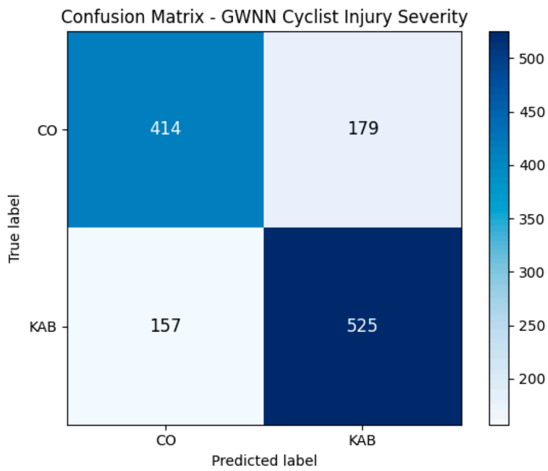

Figure A1. Confusion matrix for the GWNN model based on the binary cyclist injury severity classification.

Appendix A.3

Appendix A.3 presents the sensitivity of the GWLR model fit to alternative bandwidth specifications ranging from 1900 to 2900 nearest neighbors. The results show that model fit varies with the bandwidth choice, reflecting the trade-off between local sensitivity and spatial smoothing. Among the tested specifications, a bandwidth of 2300 provides the best overall performance, with the lowest deviance (7729.65) and AIC (7835.65), together with the highest McFadden pseudo-R^2 (0.122). Both smaller and larger bandwidths produce comparatively poorer fit, indicating that 2300 represents the most appropriate spatial scale among the evaluated alternatives. This bandwidth was therefore selected for the subsequent GWLR analysis and retained in the GWNN model to ensure consistency in the spatial weighting scale across the two geographically weighted approaches.

Table A2. GWLR model fit to alternative bandwidth specifications.

Bandwidth (Nearest Neighbors)	Deviance	AIC	McFadden Pseudo-R2
1900	7805.96	7911.96	0.113
2100	7878.17	7984.17	0.105
2300	7729.65	7835.65	0.122
2500	7968.76	8076.76	0.095
2700	8008.70	8116.70	0.090
2900	8043.66	8151.66	0.086

References

1. Younes, H.; Noland, R.B.; Von Hagen, L.A.; Sinclair, J. Cycling during and after COVID: Has there been a boom in activity? *Transp. Res. Part F Traffic Psychol. Behav.* **2023**, *99*, 71–82. [CrossRef]
2. Buehler, R.; Pucher, J. COVID-19 and cycling: A review of the literature on changes in cycling levels and government policies from 2019 to 2022. *Transp. Rev.* **2024**, *44*, 299–344. [CrossRef]
3. CDC. Bicycle Safety. Available online: https://www.cdc.gov/pedestrian-bike-safety/about/bicycle-safety.html (accessed on 20 July 2026).
4. IIHS. *Cyclists: Fatality Facts 2023*; IIHS: Ruckersville, VA, USA, 2023.

5. NCSA. *Traffic Safety Facts: Cyclists and Other Cyclists, 2023 Data*; Report No. DOT HS 813 739; U.S. Department of Transportation: Washinton, DC, USA, 2025.
6. Kim, J.K.; Kim, S.; Ulfarsson, G.F.; Porrello, L.A. Bicyclist injury severities in bicycle-motor vehicle accidents. *Accid. Anal. Prev.* **2007**, *39*, 238–251. [CrossRef]
7. Moore, D.N.; Schneider, W.H., IV; Savolainen, P.T.; Farzaneh, M. Mixed logit analysis of bicyclist injury severity resulting from motor vehicle crashes at intersection and non-intersection locations. *Accid. Anal. Prev.* **2011**, *43*, 621–630. [CrossRef]
8. Liu, J.; Khattak, A.J.; Li, X.; Nie, Q.; Ling, Z. Cyclist injury severity in traffic crashes: A spatial approach for geo-referenced crash data to uncover non-stationary correlates. *J. Saf. Res.* **2020**, *73*, 25–35. [CrossRef]
9. Dash, I.; Abkowitz, M.; Philip, C. Factors impacting bike crash severity in urban areas. *J. Saf. Res.* **2022**, *83*, 128–138. [CrossRef]
10. Dong, S.; Khattak, A.; Chen, F.; Zhou, J.B.; Xu, F.F. Analyzing severity of vehicle-bicycle crashes: An explainable boosting machine strategy. *Transp. Lett.* **2025**, *17*, 1856–1869. [CrossRef]
11. Alluri, P.; Raihan, M.A.; Saha, D.; Wu, W.; Huq, A.; Nafis, S.; Gan, A. *Statewide Analysis of Bicycle Crashes*; BDV29-977-23; Florida Department of Transportation Research Center: Tallahassee, FL, USA, 2017.
12. Raihan, M.A.; Alluri, P.; Wu, W.; Gan, A. Estimation of bicycle crash modification factors (CMFs) on urban facilities using zero inflated negative binomial models. *Accid. Anal. Prev.* **2019**, *123*, 303–313. [CrossRef]
13. Xiao, D.; Xu, X.; Duan, L. Spatial-Temporal Analysis of Injury Severity with Geographically Weighted Panel Logistic Regression Model. *J. Adv. Transp.* **2019**, *2019*, 8521649. [CrossRef]
14. Rahimi, A.; Azimi, G.; Asgari, H.; Jin, X. Injury Severity of Pedestrian and Bicyclist Crashes Involving Large Trucks. In *Proceedings of the International Conference on Transportation and Development 2020*; American Society Civil Engineers: Reston, VA, USA, 2020; pp. 110–122.
15. Hosseini, S.H.; Davoodi, S.R.; Behnood, A. Bicyclists injury severities: An empirical assessment of temporal stability. *Accid. Anal. Prev.* **2022**, *168*, 106616. [CrossRef]
16. Mannering, F.; Shankar, V.; Bhat, C.R. Unobserved heterogeneity and the statistical analysis of highway accident data. *Anal. Methods Accid. Res.* **2016**, *11*, 1–16. [CrossRef]
17. Xu, P.; Huang, H. Modeling crash spatial heterogeneity: Random parameter versus geographically weighting. *Accid. Anal. Prev.* **2015**, *75*, 16–25. [CrossRef]
18. Li, X.; Liu, J.; Zhang, Z.; Parrish, A.; Jones, S. A spatiotemporal analysis of motorcyclist injury severity: Findings from 20 years of crash data from Pennsylvania. *Accid. Anal. Prev.* **2021**, *151*, 105952. [CrossRef]
19. Zhang, Z.; Liu, J.; Li, X.; Fu, X.; Yang, C.; Jones, S. Localizing safety performance functions for two-way STOP-controlled (TWST) three-leg intersections on rural two-lane two-way (TLTW) roadways in Alabama: A geospatial modeling approach with clustering analysis. *Accid. Anal. Prev.* **2023**, *179*, 106896. [CrossRef]
20. Xu, J.; Cheung, C.; Manu, P.; Ejohwomu, O.; Too, J. Implementing safety leading indicators in construction: Toward a proactive approach to safety management. *Saf. Sci.* **2023**, *157*, 105929. [CrossRef]
21. Zafri, N.M.; Khan, A. Using geographically weighted logistic regression (GWLR) for pedestrian crash severity modeling: Exploring spatially varying relationships with natural and built environment factors. *IATSS Res.* **2023**, *47*, 325–334. [CrossRef]
22. Dormann, C.F.; Elith, J.; Bacher, S.; Buchmann, C.; Carl, G.; Carré, G.; Marquéz, J.R.G.; Gruber, B.; Lafourcade, B.; Leitao, P.J.; et al. Collinearity: A review of methods to deal with it and a simulation study evaluating their performance. *Ecography* **2013**, *36*, 27–46. [CrossRef]
23. Zhao, X.L.; Yan, X.; Yu, A.; Van Hentenryck, P. Prediction and behavioral analysis of travel mode choice: A comparison of machine learning and logit models. *Travel. Behav. Soc.* **2020**, *20*, 22–35. [CrossRef]
24. Mannering, F.; Bhat, C.R.; Shankar, V.; Abdel-Aty, M. Big data, traditional data and the tradeoffs between prediction and causality in highway-safety analysis. *Anal. Methods Accid. Res.* **2020**, *25*, 100113. [CrossRef]
25. Iranitalab, A.; Khattak, A. Comparison of four statistical and machine learning methods for crash severity prediction. *Accid. Anal. Prev.* **2017**, *108*, 27–36. [CrossRef]
26. Ali, Y.; Hussain, F.; Haque, M.M. Advances, challenges, and future research needs in machine learning-based crash prediction models: A systematic review. *Accid. Anal. Prev.* **2024**, *194*, 107378. [CrossRef]
27. Behboudi, N.; Moosavi, S.; Ramnath, R. Recent advances in traffic accident analysis and prediction: A comprehensive review of machine learning techniques. *arXiv* **2024**, arXiv:2406.13968.
28. Obasi, I.C.; Cheng, P.; Varianou-Mikellidou, C.; Dimopoulos, C.; Boustras, G. Machine learning for occupational accident analysis: Applications, challenges, and future directions. *J. Saf. Sci. Resil.* **2026**, *7*, 100250. [CrossRef]
29. Zhang, Z.; Xu, N.; Liu, J.; Jones, S. Exploring spatial heterogeneity in factors associated with injury severity in speeding-related crashes: An integrated machine learning and spatial modeling approach. *Accid. Anal. Prev.* **2024**, *206*, 107697. [CrossRef]
30. Gu, Y.; Liu, D.; Arvin, R.; Khattak, A.J.; Han, L.D. Predicting intersection crash frequency using connected vehicle data: A framework for geographical random forest. *Accid. Anal. Prev.* **2023**, *179*, 106880. [CrossRef]

31. Zhu, Y.S.; Yang, Z.Q.; Feng, X.; Cheng, C.; Guo, Y.T.; Li, Q.M.; Wu, T.H.; Li, X.H.; Witlox, F. Comparing built environment effects on bike-sharing and electric bike-sharing usage: A spatiotemporal machine learning approach. *Transp. Res. Part A Policy Pract.* **2025**, *200*, 104642. [CrossRef]
32. Cui, P.F.; Abdel-Aty, M.; Han, L.; Yang, X.B. Multiscale geographical random forest: A novel spatial ML approach for traffic safety modeling integrating street-view semantic visual features. *Transp. Res. Part C Emerg. Technol.* **2025**, *179*, 105299. [CrossRef]
33. Han, L.; Abdel-Aty, M. Intersection crash analysis considering longitudinal and lateral risky driving behavior from connected vehicle data: A spatial machine learning approach. *Accid. Anal. Prev.* **2025**, *220*, 108180. [CrossRef]
34. Kang, X.; Wu, D.X.; Sha, W.Y.; Song, K.R.; Wang, S.Q. Analysis and Prediction of Traffic Accidents Based on Interpretable Spatial Machine Learning: A Case Study in California. *J. Adv. Transp.* **2025**, *2025*, 3184284. [CrossRef]
35. Mostafa, A.M.; Aldughayfiq, B.; Tarek, M.; Alaerjan, A.S.; Allahem, H.; Elbashir, M.K.; Ezz, M.; Hamouda, E. AI-based prediction of traffic crash severity for improving road safety and transportation efficiency. *Sci. Rep.* **2025**, *15*, 27468. [CrossRef]
36. Isaksson-Hellman, I.; Toreki, J. The effect of speed limit reductions in urban areas on cyclists' injuries in collisions with cars. *Traffic Inj. Prev.* **2019**, *20*, 39–44. [CrossRef]
37. Macioszek, E.; Granà, A. The Analysis of the Factors Influencing the Severity of Bicyclist Injury in Bicyclist-Vehicle Crashes. *Sustainability* **2022**, *14*, 215. [CrossRef]
38. Phuksuksakul, N.; Haque, M.; Yasmin, S. The role of posted speed limit on pedestrian and bicycle injury severities: An investigation into systematic and unobserved heterogeneities. *Anal. Methods Accid. Res.* **2024**, *44*, 100351. [CrossRef]
39. SafeTREC. 2025 Series of SafeTREC Traffic Safety Facts Released! UC Berkeley SafeTREC. Available online: https://safetrec.berkeley.edu/news/2025-series-safetrec-traffic-safety-facts-released-0 (accessed on 3 April 2026).
40. Liu, J.; Khattak, A.J. Are gates at rail grade crossings always safe? Examining motorist gate-violation behaviors using path analysis. *Transp. Res. Part F Traffic Psychol. Behav.* **2018**, *55*, 314–324. [CrossRef]
41. Scarano, A.; Sadeghi, M.; Mauriello, F.; Riccardi, M.R.; Aghabayk, K.; Montella, A. Cyclist crash severity modeling: A hybrid approach of XGBoost-SHAP and random parameters logit with heterogeneity in means and variances. *J. Saf. Res.* **2025**, *93*, 373–398. [CrossRef]
42. Liu, J.; Khattak, A.J.; Chen, C.; Wan, D.; Ma, J.Q.; Hu, J. Revisiting Hit-and-Run Crashes: A Geo-Spatial Modeling Method. *Transp. Res. Rec.* **2018**, *2672*, 81–92. [CrossRef]
43. Azimi, S. Investigating the Effect of Road Characteristics on Pedestrian and Bike Crash Frequency. Master's Thesis, University of Hawai'i at Manoa, Honolulu, HI, USA, 2024.
44. Lu, W.; Liu, J.; Fu, X.; Yang, J.; Jones, S. Integrating machine learning into path analysis for quantifying behavioral pathways in bicycle-motor vehicle crashes. *Accid. Anal. Prev.* **2022**, *168*, 106622. [CrossRef]
45. Wahi, R.R.H.; Haworth, N.; Debnath, A.K.; King, M. Influence of Type of Traffic Control on Injury Severity in Bicycle-Motor Vehicle Crashes at Intersections. *Transp. Res. Rec.* **2018**, *2672*, 199–209. [CrossRef]
46. Chandia-Poblete, D.; Hill, R.L.; Aguilar-Farias, N.; Heesch, K.C. Individual and contextual factors associated with bicyclist injury severity in traffic incidents between bicyclists and motorists in Chile. *Accid. Anal. Prev.* **2021**, *154*, 106077. [CrossRef]
47. Dozza, M. Crash risk: How cycling flow can help explain crash data. *Accid. Anal. Prev.* **2017**, *105*, 21–29. [CrossRef]
48. Liu, S.J.; Li, Y.; Fan, W. Mixed logit model based diagnostic analysis of bicycle-vehicle crashes at daytime and nighttime. *Int. J. Transp. Sci. Technol.* **2022**, *11*, 738–751. [CrossRef]
49. Samerei, S.A.; Aghabayk, K.; Shiwakoti, N.; Mohammadi, A. Using latent class clustering and binary logistic regression to model Australian cyclist injury severity in motor vehicle-bicycle crashes. *J. Saf. Res.* **2021**, *79*, 246–256. [CrossRef]
50. Lin, H.A.; Chan, C.W.; Wiratama, B.S.; Chen, P.L.; Wang, M.H.; Chao, C.J.; Saleh, W.; Huang, H.C.; Pai, C.W. Evaluating the effect of drunk driving on fatal injuries among vulnerable road users in Taiwan: A population-based study. *BMC Public Health* **2022**, *22*, 2059. [CrossRef]
51. Chao, C.C.; Ma, H.P.; Wei, L.; Lin, Y.N.; Chen, C.; Saleh, W.; Wiratama, B.S.; Widodo, A.F.; Hsu, S.C.; Ko, S.Y.; et al. Risk factors for overtaking, rear-end, and door crashes involving bicycles in the United Kingdom: Revisited and reanalysed. *PLoS ONE* **2025**, *20*, e0315692. [CrossRef]
52. Hargrove, I. Injury Severity Assessment of Bicycle Crashes on Rural Roadways in Wisconsin. Doctoral Dissertation, University of Wisconsin-Madison, Madison, WI, USA, 2025.
53. Janstrup, K.H.; Kostic, B.; Moller, M.; Rodrigues, F.; Borysov, S.; Pereira, F.C. Predicting injury-severity for cyclist crashes using natural language processing and neural network modelling. *Saf. Sci.* **2023**, *164*, 106153. [CrossRef]
54. Asgarzadeh, M.; Fischer, D.; Verma, S.K.; Courtney, T.K.; Christiani, D.C. The impact of weather, road surface, time-of-day, and light conditions on severity of bicycle-motor vehicle crash injuries. *Am. J. Ind. Med.* **2018**, *61*, 556–565. [CrossRef]
55. Yuan, C.; Li, Y.; Huang, H.; Wang, S.; Sun, Z.; Wang, H. Application of explainable machine learning for real-time safety analysis toward a connected vehicle environment. *Accid. Anal. Prev.* **2022**, *171*, 106681. [CrossRef]
56. Bil, M.; Bilova, M.; Muller, I. Critical factors in fatal collisions of adult cyclists with automobiles. *Accid. Anal. Prev.* **2010**, *42*, 1632–1636. [CrossRef]

57. Soroori, E.; Mohammadzadeh Moghaddam, A.; Salehi, M. Modeling spatial nonstationary and overdispersed crash data: Development and comparative analysis of global and geographically weighted regression models applied to macrolevel injury crash data. *J. Transp. Saf. Secur.* **2021**, *13*, 1000–1024. [CrossRef]
58. Anastasopoulos, P.; Mannering, F.L. A note on modeling vehicle accident frequencies with random-parameters count models. *Accid. Anal. Prev.* **2009**, *41*, 153–159. [CrossRef]
59. Adanu, E.K.; Hainen, A.; Jones, S. Latent class analysis of factors that influence weekday and weekend single-vehicle crash severities. *Accid. Anal. Prev.* **2018**, *113*, 187–192. [CrossRef]
60. Chun, U.; Lim, J.; Lee, S.; Park, S. An analysis of bicycle accidents with respect to spatial heterogeneity. *Sci. Rep.* **2023**, *13*, 21812. [CrossRef]
61. Fotheringham, A.S.; Charlton, M.E.; Brunsdon, C. Geographically weighted regression: A natural evolution of the expansion method for spatial data analysis. *Environ. Plan. A* **1998**, *30*, 1905–1927. [CrossRef]
62. Li, Z.Q. Extracting spatial effects from machine learning model using local interpretation method: An example of SHAP and XGBoost. *Comput. Environ. Urban. Syst.* **2022**, *96*, 101845. [CrossRef]
63. Molnar, C. *Interpretable Machine Learning*; Leanpub: Victoria, BC, Canada, 2020.
64. Scarano, A.; Rella Riccardi, M.; Mauriello, F.; D'Agostino, C.; Pasquino, N.; Montella, A. Injury severity prediction of cyclist crashes using random forests and random parameters logit models. *Accid. Anal. Prev.* **2023**, *192*, 107275. [CrossRef]
65. Goswamy, A.; Abdel-Aty, M.; Islam, Z. Factors affecting injury severity at pedestrian crossing locations with Rectangular RAPID Flashing Beacons (RRFB) using XGBoost and random parameters discrete outcome models. *Accid. Anal. Prev.* **2023**, *181*, 106937. [CrossRef]
66. Yuan, T.; Da Rocha Neto, W.; Rothenberg, C.E.; Obraczka, K.; Barakat, C.; Turletti, T. Machine learning for next-generation intelligent transportation systems: A survey. *Trans. Emerg. Telecommun. Technol.* **2022**, *33*, e4427. [CrossRef]
67. Li, J.; Wang, X.; Yang, X.; Zhang, Q.; Pan, H. Analyzing freeway safety influencing factors using the CatBoost model and interpretable machine-learning framework, SHAP. *Transp. Res. Rec.* **2024**, *2678*, 563–574. [CrossRef]
68. Putra, I.G.B.; Kuo, P.F.; Susanta, F.F.; Tedjo, B.H.; Lord, D. GeoShapley-based interpretation of older adult pedestrian fatal vs injury crash frequency in dense urban environments. *Accid. Anal. Prev.* **2026**, *230*, 108450. [CrossRef]
69. NCDOT. *NCDOT Cyclist and Pedestrian Crash Map*; North Carolina Department of Transportation: Raleigh, NC, USA, 2024.
70. FHWA. KABCO Injury Classification Scale and Definitions. Available online: https://safety.fhwa.dot.gov/hsip/spm/conversion_tbl/pdfs/kabco_ctable_by_state.pdf (accessed on 8 August 2026).
71. FHWA. *Focusing on Crash Severity in HSIP Project Selection*; U.S. Department of Transportation: Washington, DC, USA, 2015.
72. Behrooz, H.; Hayeri, Y.M. Machine Learning Applications in Surface Transportation Systems: A Literature Review. *Appl. Sci.* **2022**, *12*, 9156. [CrossRef]
73. Dougherty, M. A Review of Neural Networks Applied to Transport. *Transp. Res. Part C Emerg. Technol.* **1995**, *3*, 247–260. [CrossRef]
74. Islam, M.; Chen, G.; Jin, S. An overview of neural network. *Am. J. Neural Netw. Appl.* **2019**, *5*, 7–11. [CrossRef]
75. Liu, R.; Shin, S.Y. A Review of Traffic Flow Prediction Methods in Intelligent Transportation System Construction. *Appl. Sci.* **2025**, *15*, 3866. [CrossRef]
76. Goodfellow, I.; Bengio, Y.; Courville, A.; Bengio, Y. *Deep Learning*; MIT Press Cambridge: Cambridge, MA, USA, 2016; Volume 1.
77. Zeng, Q.; Huang, H. A stable and optimized neural network model for crash injury severity prediction. *Accid. Anal. Prev.* **2014**, *73*, 351–358. [CrossRef]
78. Zeng, Q.; Huang, H.L.; Pei, X.; Wong, S.C. Modeling nonlinear relationship between crash frequency by severity and contributing factors by neural networks. *Anal. Methods Accid. Res.* **2016**, *10*, 12–25. [CrossRef]
79. Jamal, A.; Umer, W. Exploring the Injury Severity Risk Factors in Fatal Crashes with Neural Network. *Int. J. Environ. Res. Public Health* **2020**, *17*, 7466. [CrossRef]
80. Shen, X.; Wei, S. Severity analysis of road transport accidents of hazardous materials with machine learning. *Traffic Inj. Prev.* **2021**, *22*, 324–329. [CrossRef]
81. Zhang, Z.; Nie, Q.; Liu, J.; Hainen, A.; Islam, N.; Yang, C. Machine learning based real-time prediction of freeway crash risk using crowdsourced probe vehicle data. *J. Intell. Transp. Syst.* **2024**, *28*, 84–102. [CrossRef]
82. Adanu, E.K.; Su, Y.; Khan, S.H.; Penmetsa, P.; Zhang, Z.; Jones, S. The safety risks of roadside trees: An analysis of injury outcomes in vehicle-tree collisions. *Accid. Anal. Prev.* **2026**, *238*, 108751. [CrossRef]
83. Liu, J.; Khattak, A.J. Gate-violation behavior at highway-rail grade crossings and the consequences: Using geo-Spatial modeling integrated with path analysis. *Accid. Anal. Prev.* **2017**, *109*, 99–112. [CrossRef]
84. Liu, J.; Jones, S.; Adanu, E.K.; Li, X. Behavioral pathways in bicycle-motor vehicle crashes: From contributing factors, pre-crash actions, to injury severities. *J. Saf. Res.* **2021**, *77*, 229–240. [CrossRef]
85. Xu, N.Z.; Liu, J.; Zhang, Z.H.; Jones, S. Injury severity of police officers involved in traffic crashes: A spatial analysis of Alabama. *Saf. Sci.* **2024**, *172*, 106406. [CrossRef]
86. Miller, H.J. Tobler's first law and spatial analysis. *Ann. Assoc. Am. Geogr.* **2004**, *94*, 284–289. [CrossRef]

87. Fotheringham, A.S.; Brunsdon, C.; Charlton, M. *Geographically Weighted Regression*; Wiley: Hoboken, NJ, USA, 2009.
88. Boele-Vos, M.J.; Van Duijvenvoorde, K.; Doumen, M.J.A.; Duivenvoorden, C.; Louwerse, W.J.R.; Davidse, R.J. Crashes involving cyclists aged 50 and over in the Netherlands: An in-depth study. *Accid. Anal. Prev.* **2017**, *105*, 4–10. [CrossRef]
89. Helak, K.; Jehle, D.; McNabb, D.; Battisti, A.; Sanford, S.; Lark, M.C. Factors influencing injury severity of cyclists involved in crashes with motor vehicles: Bike lanes, alcohol, lighting, speed, and helmet use. *South. Med. J.* **2017**, *110*, 441–444. [CrossRef]
90. Behnood, A.; Mannering, F. Determinants of cyclist injury severities in bicycle-vehicle crashes: A random parameters approach with heterogeneity in means and variances. *Anal. Methods Accid. Res.* **2017**, *16*, 35–47. [CrossRef]
91. Jones, D.L. The Behavioral Impacts of Urban Street Modifications: A Case Study of East Blvd. in Charlotte. Doctoral Dissertation, North Carolina State University, Raleigh, NC, USA, 2012.
92. Haworth, N.; Schramm, A. The safety of bicycles being overtaken by cars: What do we know and what do we need to know? In Proceedings of the 2014 Australasian Road Safety Research, Policing & Education Conference, Melbourne, Australia, 12–14 November 2014.
93. Wang, C.; Lu, L.; Lu, J. Statistical analysis of cyclists' injury severity at unsignalized intersections. *Traffic Inj. Prev.* **2015**, *16*, 507–512. [CrossRef]
94. Thomas, L.; Ryus, P.; Semler, C.; Thirsk, N.J.; Krizek, K.J.; Zegeer, C.V. *Delivering Safe, Comfortable, and Connected Pedestrian and Bicycle Networks: A Review of International Practices*; FHWA-15-051; U.S. Department of Transportation: Washington, DC, USA, 2015.
95. NTSB. *Cyclist Safety on US Roadways: Crash Risks and Countermeasures*; National Transportation Safety Board: Washington, DC, USA, 2019.
96. FHWA. *Speed Management Countermeasures: More than Just Speed Humps*; U.S. Department of Transportation: Washington, DC, USA, 2017.
97. Schultheiss, B.; Goodman, D.; Blackburn, L.; Wood, A.; Reed, D.; Elbech, M. *Bikeway Selection Guide*; U.S. Department of Transportation: Washington, DC, USA, 2019.
98. Islam, S.; Hossain, A.B. Comparative Analysis of Injury Severity Resulting from Pedestrian-Motor Vehicle and Bicycle-Motor Vehicle Crashes on Roadways in Alabama. *Transp. Res. Rec.* **2015**, *2514*, 79–87. [CrossRef]
99. Reynolds, C.C.; Harris, M.A.; Teschke, K.; Cripton, P.A.; Winters, M. The impact of transportation infrastructure on bicycling injuries and crashes: A review of the literature. *Environ. Health* **2009**, *8*, 47. [CrossRef]
100. Beyer, F.R.; Ker, K. Street lighting for preventing road traffic injuries. *Cochrane Database Syst. Rev.* **2009**, *2009*, CD004728. [CrossRef]
101. Dai, B.; Wang, X.; Guo, Q.; Yang, L.; Bai, Y. Safety evaluation of protected bike lane treatments at intersections: A causal framework. *Accid. Anal. Prev.* **2025**, *220*, 108132. [CrossRef]
102. Paterson, G.; Atanda-Ogunleye, O.; Higgins, E.; Pearson, B. Reducing Motor Vehicle Crashes Involving Pedestrians and Cyclists in North Carolina. Master's Thesis, University of North Carolina at Chapel Hill, Chapel Hill, NC, USA, 2024.
103. Charyk Stewart, T.; Pellar, A.; Halari, M.; McClafferty, K.; Verville, P.; Pickup, M.; Fraser, D.; Gilliland, J.; Shkrum, M. Safe system approach to preventing cyclist fatalities: Safety by design for urban and rural environments. *Inj. Epidemiol.* **2025**, *12*, 71. [CrossRef]
104. FHWA. *Lighting: Proven Safety Countermeasures*; U.S. Department of Transportation: Washington, DC, USA, 2021.
105. Pucher, J.; Buehler, R. Safer Cycling Through Improved Infrastructure. *Am. J. Public Health* **2016**, *106*, 2089–2091. [CrossRef]
106. Sundstrom, C.A.; Quinn, S.M.; Weld, R. Cyclist crash comparison of mixing zone and fully split phase signal treatments at intersections with protected bicycle lanes in New York City. *Transp. Res. Rec.* **2019**, *2673*, 115–124. [CrossRef]
107. FHWA. *Systemic Safety Project Selection Tool*; FHWA-SA-13-019; U.S. Department of Transportation, Federal Highway Administration, Office of Safety: Washington, DC, USA, 2013.
108. ConnectNCDOT. Complete Streets. Available online: https://connect.ncdot.gov/projects/BikePed/Pages/Complete-Streets.aspx (accessed on 20 July 2026).
109. ConnectNCDOT. Bicycle & Pedestrian Project Development & Design Guidance. Available online: https://connect.ncdot.gov/projects/BikePed/Pages/Guidance.aspx (accessed on 6 July 2026).
110. Jevremović, S.; Trpković, A.; Čičević, S.; Čubranić Dobrodolac, M.; Kachadoorian, C. Age-Friendly Cycling Infrastructure—Differences and Preferences among 50+ Cyclists. *Sustainability* **2024**, *16*, 7280. [CrossRef]